05

Regional Sea Level Changes Projected by the NASA/GISS Atmosphere-Ocean Model

Gary L. Russell, Vivien Gornitz, and James R. Miller

NASA / Goddard Institute for Space Studies
2880 Broadway
New York, NY 10025
USA

Submitted to Climate Dynamics: 1999 November 19

E-mail address: grussell@giss.nasa.gov

Abstract

Sea level has been rising for the past century, and inhabitants of the Earth's coastal regions will want to understand and predict future sea level changes. In this study we present results from new simulations of the Goddard Institute for Space Studies (GISS) global atmosphere-ocean model from 1950 to 2099. Model results are compared with observed sea level changes during the past 40 years at 17 coastal stations around the world. Using observed levels of greenhouse gases between 1950 and 1990 and a compounded 0.5% annual increase in CO_2 after 1990, model projections show that global sea level measured from 1950 will rise by 61 mm in the year 2000, by 212 mm in 2050, and by 408 mm in 2089. By 2089, two thirds of the global sea level rise will be due to thermal expansion and one third will be due to ocean mass changes. The spatial distribution of sea level rise is different than that projected by rigid lid ocean models.

1. Introduction

During the last century, sea level has been rising throughout much of the world at rates between 1 and 2.5 mm/year with a best estimate of 1.8 mm/year [Warrick et al., 1996; Gornitz, 1995a]. Increasing levels of atmospheric greenhouse gases are mainly responsible for the present global sea level rise and its future continuation. There are two major components to long term sea level changes: first, water expands as ocean temperatures change and salt is redistributed; and second, land ice stored on the continents and in polar ice sheets melts and flows into the oceans. At any coastal location, vertical land motions may also affect local mean sea level. Locally, we will use the term "steric expansion" for a combination of thermal and haline expansion; whereas globally, we will simply use "thermal expansion" because the global effect of haline expansion is negligible.

Several prior studies have modeled potential changes in sea level in coupled atmosphere-ocean models. Gregory [1993] forced a U.K. Meteorological Office model, that had a climate sensitivity of 2.7°C for doubled CO_2, with 1% annual increases of CO_2. He estimated a sea level rise of 90 mm due to thermal expansion alone after 70 years. Cubasch et al. [1995] coupled the atmospheric component (ECHAM-1) and the large scale geostrophic ocean model (LSG) in a warm start simulation with the radiative forcing of Scenario A ("Business as Usual") from the Intergovernmental Panel on Climate Change (IPCC). The global sea level rise due to thermal expansion was 180 mm after 100 years. In a companion cold start simulation, the sea level rise was only 150 mm. Bryan [1996] used the Geophysical Fluid Dynamics Laboratory coupled model in a 1% CO_2 annual increase simulation. After 70 years, global sea level rose 150 mm due to thermal expansion alone. None of these models calculates sea level directly by vertically integrating specific volume with respect to mass per unit area. Their derivations are more complicated because they require the surface pressure, the surface stress, and ocean variables.

Other studies have used one or two dimensional models to

examine both thermal expansion and water mass changes that cause sea level to rise. Raper et al. [1996] combined a simple one dimensional upwelling-diffusion energy balance model to a set of simple ice-melt models in order to compute total sea level change. Using the IPCC 1995 suite of greenhouse gas emissions scenarios [Houghton et al., 1996], they found a sea level rise of 200-860 mm from year 1990 to 2100, with a mid value of 490 mm for a climate sensitivity of 2.5°C for doubled CO_2. De Wolde et al. [1997] applied a two dimensional energy balance climate model and dynamic ice sheet models to the IPCC forcing scenarios to estimate sea level rise contributions from thermal expansion and glacial melting. Their results were considerably lower than those of the IPCC [Warrick et al., 1996]. Sea level rise projections showed a strong sensitivity to differences in model features.

In this study, we use the global coupled atmosphere-ocean model of Russell et al. [1995] to examine sea level rise between 1950 and 2099. The model conserves global water mass in all phases and calculates the ocean surface height by integrating specific volume with respect to mass from the ocean floor. The model is described in section 2. Four 150-year model simulations used in the analysis are discussed in section 3. In section 4, the results are compared with observed changes from 1960 to 1997. In section 5, the model is used to project sea level changes through to the end of the twenty first century. A breakdown of the water mass changes is performed in section 6.

2. The NASA/GISS atmosphere-ocean model

The global synchronously coupled atmosphere-ocean model developed by Russell et al. [1995] is designed for climate studies on decade to century time scales. There are nine vertical layers in the atmosphere and 13 in the ocean. The horizontal resolution for both the atmosphere and ocean is 4° in latitude by 5° in longitude. The resolution for heat, water vapor, and salt is finer than the grid resolution because those quantities have both means and directional prognostic gradients

inside each grid cell. This information is used in the advection by the linear upstream scheme, and atmospheric condensation and ocean vertical mixing are performed on 2° x 2.5° horizontal resolution. The model does not use flux adjustments.

Several changes and improvements have been made to the model since it was published. The ground hydrology scheme of Abramopoulos et al. [1988] is now implemented, land ice and sea ice coding uses four thermodynamic layers, sea ice is advected, glacial ice calving is implemented off Antarctica, and the k-profile parameterization (KPP) scheme [Large et al., 1994] is used for ocean vertical mixing. Before the KPP scheme was implemented, the equilibrium surface air temerature change due to doubled CO_2 was estimated to be 2.65°C [Andrei Sokolov and Peter Stone, personal communication].

The ocean model does not use the Boussinesq approximation, and ocean mass, not volume, is conserved. As part of the ocean pressure gradient force, altitude is calculated by integrating the local specific volume with respect to mass per unit area from the ocean floor. The specific volume is calculated with quadratic precision in each layer using the mean and vertical gradients of heat and salt. The ocean surface height, which is sampled each hour, is the summation of the liquid ocean surface height plus the snow and sea ice mass per unit area divided by a constant density of 1000 kg/m^3 which measures the freshwater equivalent of snow and ice.

Ocean mass decreases due to evaporation and increases due to precipitation, river flow including melted ice, and glacial ice calving from Antarctica. Snow over ground increases indefinitely at certain cold grid cells. Continual long term changes of water mass between a control simulation and a GHG experiment over ground are mainly due to snow changes because canopy and underground water storage is limited. Glacial ice reservoirs, which are fixed in area, can melt or accumulate ice indefinitely, but the changes are captured by the model's diagnostics. Negative lake mass changes may occur by excessive evaporation from the surface area of a lake that does not receive sufficient precipitation, source runoff from within its grid cell, or river

flow from upstream lakes. Positive lake mass changes may occur when water sources exceed evaporation (the surface area may be negligible) and there is no or slow outgoing river flow. In the model, lakes occupy 0.8% of the global surface area and are fixed.

3. Model simulations

Four simulations of the atmosphere-ocean model from 1950 to 2099 are used in this study: two control simulations with constant 1950 atmospheric composition that differ only in their initial conditions; and two GHG experiments with observed greenhouse gases until 1990 and 0.5% compounded annual increases of CO_2 after 1990. In addition, two GHG+SO4 experiments with varying tropospheric sulfate aerosols were run; but because their temperature comparisons did not agree as well with observations as did the GHG experiments [Russell et al., 1999], they have not been included here. The radiative forcing of 0.5% CO_2 increases is in line with the radiative forcing of all greenhouse gas increases for the past few years [Hansen et al., 1998]. The initial conditions are 40-year and 100-year spinups with constant 1950 atmospheric composition starting from Levitus et al. [1994] ocean state. In order to minimize climate drift (continual accumulation of heat or salt at certain locations) and deviations from observations, model climate changes are calculated as an experiment minus a control simulation.

Russell et al. [1999] compared these current simulations with the observed regional temperature record of the past 40 years and concluded that the model faithfully represents the real world's regional climate changes due to greenhouse gas forcing in the northern hemisphere. They estimated that the unrealized warming in surface air temperature due to the cold start initialization is 0.23°C, but because the 1930s and 1940s were anomalously warm decades, the surface air temperature disparity with observations is negligible. Although the cold start initialization may not be detectable in the surface air temperature, it should be present in the deep ocean temperatures

and ocean surface height. Consequently, the model's sea level changes probably underestimate those that occur in the real world.

The northern hemisphere sea ice cover compares well with observations. The southern hemisphere sea ice cover is stable with a seasonal range that is in good agreement with observations, but the interannual variability is much greater than observed. This is a major factor that prevents the model's regional temperature changes from matching the observational changes for the past 40 years in the southern hemisphere.

4. Model and observed sea level trends from 1960 to 1997

Monthly raw tide gauge data are obtained from the Permanent Service for Mean Sea Level (PSMSL) data base [Spencer and Woodworth, 1993]. Some records go back more than 100 years, but most records are too short or too broken to be useful for sea level studies [Gornitz, 1995a]. A small subset of 17 tide gauge stations were selected for comparison with model generated sea level curves. These stations were chosen on the basis of record length, geographical coverage, and availability of adequate geologic data [Gornitz, 1995b; Gornitz and Solow, 1991; Gornitz and Lebedeff, 1987; Pirazzoli, 1991]. Missing monthly tide guage data are filled in by interpolation between the same months in prior and subsequent years with a maximum gap of two missing years. Annual data are calculated whenever original or filled in data are available for all 12 months; otherwise an annual data gap occurs.

For each station, tide gauge annual values are normalized by calculating a 21 year mean, centered on 1950, and then subtracting this mean from each annual value. Finally, the geologic trend or vertical land motion is subtracted from the normalized annual values to obtain the corrected sea level change relative to 1950 that can be compared with model results.

Sea level data recorded by tide gauges include long term trends caused by vertical crustal motions largely of glacial

isostatic or tectonic origin [Peltier and Tushingham, 1991; Gornitz, 1995a,b]. The late Holocene (past 6000 years) sea level curve constructed from fossil tide level indicators, such as peat, coral, in-situ shells, barnacles, etc., represents a composite of these long term geologic components. The long term geologic motion can be approximated by a linear trend over the relatively short time periods considered here. By differencing the modern and late Holocene sea level curves, the residual provides a measure of the recent sea level rise due to global warming [Gornitz, 1995b].

Table 1 lists the station names, latitude, longitude, years of record, the raw tide gauge trend (mm/year) for all years of the record, the geologic trend due to land motions, the corrected tide gauge trend for all years of the record, the corrected tide gauge trend for years 1960 to present, and the model sea level trends for each GHG experiment from 1960 until the end of the observational record. The trends are calculated as the slope of the least squares fit line through the annual sea level data. Note the negative geologic trends in Table 1 at Churchill on Hudson Bay, Stavanger in Norway, and Stockholm which are undergoing glacial isostatic uplift, and the positive values at Halifax and New York City due to subsidence of the collapsed forebulge [Peltier and Tushingham, 1991; Peltier, 1999].

For each of the 17 stations, Figure 1 shows the sea level changes for all years of the corrected tide gauge data and for 1960 to 2089 of each GHG experiment. For Figures 1 and 2, a GHG data point consists of a GHG annual value minus a centered 21 year moving average of the control simulation values. Subtracting control simulation values reduces the effects of climate drift, and the 21 year averaging period lets the GHG data show its proper interannual variability.

Table 1 shows that between 1960 and 1997 the models' sea level trends are positive at all 17 stations and are generally greater than the corrected tide gauge trends. The global mean sea level trends of 1.41 and 1.34 mm/year for the two GHG experiments between 1960 and 1997 fall within the observed range [Warrick et al., 1996; Gornitz, 1995a], but the average of the

corrected tide gauge trends lie below this range due to the limited sampling of the 17 stations reported here. Two stations, Balboa and Churchill, with negative corrected tide gauge trends since 1960, have anomalous data points (see Figure 1). At two other stations, Halifax and Marseille, the corrected tide gauge trends are negative since 1960, but are positive for the entire record dating back to 1920 and 1885 respectively. This points to the importance of using stations with long record lengths [Douglas, 1995].

In general, the model's interannual variability appears to be less than that of the observations, but stations with large model variability also display large observational variability, e.g. Prince Rupert and Stockholm (see Figure 1). A large source of interannual variability in sea level data comes from the El Nino-Southern Oscillation (ENSO) [Nerem, 1999] or the North Atlantic Oscillation (NAO) [Hurrell,1995]. ENSO and NAO anomalies appear in tide gauge records [Komar and Enfield,1987; Maul and Hanson, 1991; Gornitz, unpublished data].

The sharp positive spike in 1982 in the San Francisco sea level curve (Figure 1m) is related to ENSO, as are lesser anomalies in 1941, 1958, 1969 and 1972. The sharp positive sea level anomaly in 1983 in the Buenos Aires sea level curve (also in Montevideo, Uruguay and in more subdued form in the Mar del Plata and Puerto Madryn, Argentina records) may also be linked indirectly to ENSO. Both the Buenos Aires and Montevideo records are strongly influenced by river flow from the Parana and Uruguay Rivers, which may have been above normal due to higher than average precipitation. On the other hand, ENSO impacts are harder to explain for the two more southerly coastal stations.

5. Modeled sea level changes to the year 2099

Figure 2 shows the temporal change in global sea level from 1960 to 2089 for the two GHG experiments minus the controls. It also shows the fractions due to thermal expansion and to water mass changes.

These data are also recorded in Table 2 in a format consistent with Table 3. The fourth line of Table 2, shows the difference in heat that enters the ocean between the GHG experiments and the control simulations. The ratio of global sea level rise due to thermal expansion (mm/year) divided by the heat entering the ocean (W/m^2) gives the "expansion efficiency of heat" ($m^3/kW \cdot year$), the final line of Table 2. Note that the model's expansion efficiency for the first 50 years was greater than for the next century. As the warming penetrates more deeply into colder waters, the expansion is less efficient.

The expansion efficiency of heat can be calculated from known ocean variables [Fofonoff and Millard, 1983] as the derivative of specific volume with respect to temperature ($m^3/kg°C$) divided by specific heat capacity ($J/kg°C$). Figure 3 shows the expansion efficiency as a function of temperature and pressure at a salinity of 35 per mil. The expansion efficiency of heat increases with temperature, pressure or salinity.

Bryan [1996] provided a rough estimate of an additional 3 W/m^2 entering his model's ocean for years 50 to 70 in his 1% CO_2 experiment. From his Figure 2a, we estimate a sea level rise due to thermal expansion of 3.47 mm/year for those two decades which translates into an expansion efficiency of 1.16 $m^3/kW \cdot year$. Either his heating rate is only approximate, or his heat is penetrating into colder waters than in our experiments.

Figure 4 shows the spatial distribution of projected sea level rise for 2050 to 2099 minus 1950. It was calculated as the 50 year average of the two GHG experiments minus the 50 year average of the two control simulations. The largest rise in sea level occurs in the Arctic Ocean where increased river flow (due to increased precipitation) and decreased sea ice export cause the salinity to decrease and the specific volume to increase. Small rises occur near the Antarctic Circumpolar Current where there is less deposition of sea ice (causing salinity to increase), where temperatures are cold (reducing the expansion efficiency of heat), and where less ocean heat transport is received (due to a slowing of the ocean circulation).

Gregory [1993] and Bryan [1996] employ similar rigid lid ocean models and their complicated calculations of sea level changes produce similar spatial patterns. The present study and that of Cubasch et al. [1995] show spatial patterns of sea level rise that differ between each other and differ from those of Gregory and Bryan. Both Bryan's and our results show the greatest rise in the Arctic Ocean and small rises in the center of the North Atlantic and near Antarctica. Our model shows low rises in the north Pacific and high rises in the tropical Pacific which are opposite to that shown by Bryan.

Figure 5 shows the model's projected sea level rise due to steric expansion for 2050 to 2099 minus 1950. It is calculated as the difference between the total sea level rise (Figure 4) minus the rise due to water mass changes (Figure 6) using the average of the two GHG experiments and the two control simulations. The steric expansion is small over shallow seas where there is less water to heat and over areas where the reduced ocean circulation is depositing less heat. The greatest changes occur in the deep basins of the Arctic Ocean due to less saline water.

6. Storage changes in water reservoirs

The atmosphere-ocean model does not include anthropogenic modifications of land hydrology, such as dams, river diversions, or ground water withdrawals, which may affect sea level [Gornitz et al., 1997]. The glacial ice calving from Antarctica is constant in the model and cannot affect the model's sea level changes. On the other hand, the repartition of water among the model's reservoirs does cause sea level changes.

Figure 6 shows the model's projected ocean water mass changes for 2050 to 2099 minus 1950. High values occur over shallow ocean areas where steric expansion contributes a proportionally smaller share to global sea level, because of the thinner water column. Negative values occur, particularly in the

deep areas of the Arctic Ocean, where increased freshwater input reduces the salinity and greater haline expansion is pushing mass out.

Table 3 shows the mass changes in the model's water reservoirs for each 50-year period and for each GHG experiment minus its control simulation. Volumetric changes are calculated in units of global sea level rise (mm/year) by dividing the annual change in a reservoir (kg/year) by the product of density (1000 kg/m^3) times ocean and sea ice surface area (361e+12 m^2). As the climate warms, atmospheric water vapor, lake mass, and ocean mass increase at the expense of land ice and snow.

Figure 7 shows the changes in water or ice accumulation in the continental reservoirs for 2050 to 2099 minus 1950. The net mass balance of land ice is negative in both hemispheres, on average: melting rapidly in the northern hemisphere but slowly in Antarctica. The coastal regions of Greenland are losing mass, even though precipitation is increasing almost everywhere there. Snow and ice are also melting in Alaska and the Himalayas. The high altitude coastal regions and interior of Antarctica are slowly accumulating snow, whereas the ice shelves are melting rapidly.

There are significant changes in some grid cells that do not drain to the ocean. Lake Turkana in Kenya, Somalia, and western Mongolia are receiving more water in the GHG experiments, whereas Lakes Titicaca and Poopo in the Andes, the Aral Sea, Afghanistan, and southern Ethiopia are receiving less. There are also increasing lake levels in regions with slow moving rivers, namely Parana tributaries in southern Brazil, the Zambezi mouth, and the headwaters of the Zaire River. Changes at individual grid cells are uncertain; they should be checked with ground observations and other data.

7. Discussion

Four simulations of the NASA/GISS atmosphere-ocean model are used to emulate sea level changes between 1950 and 1997, and to project such changes to the year 2099. The only radiative forcing used is that of greenhouse gas changes: observed concentrations were used before 1991 and a compounded annual increase of 0.5% for CO_2 was used from 1991 to 2099. The simulations predict that global sea level will rise at a rate of 1.23 mm/year between 1950 and 1999, going to 2.97 between 2000 and 2049, and to 5.21 between 2050 and 2099. Because the GHG experiments are started from equilibrium, they underestimate the sea level rise that should have occurred in the real world since the real world was not in equilibrium in 1950. Observations indicate that during the past century sea level has risen between 1 and 2.5 mm/year [Warrick et al., 1996]. Uncertainies in future greenhouse gas concentrations introduce uncertainies into the model's prediction of future sea level rise.

The surface air temperature changes of these simulations have been compared to observed temperature changes for the past 40 years and have been found to be reasonable both globally and regionally in the northern hemisphere [Russell et al., 1999]. The thermal expansion component of sea level is controlled mainly by ocean surface fluxes and by ocean mixing both of which also affect the surface air temperature. Consequently, we expect the the ocean thermal expansion in the model to be reasonable.

Global thermal expansion rates from different one dimensional, two dimensional, and three dimensional models are difficult to compare. Ideally, a model report on sea level rise should provide three key pieces of information on thermal expansion: the forcing scenario used, the amount of heat that entered the ocean, and the global sea level rise due to that heat. The second piece is often omitted, but were it to be provided (and it should be available), it would break a complex process into two simpler processes.

A new term, the "expansion efficiency of heat", which is the ratio of sea level rise due to thermal expansion divided by the

heat entering the ocean, can be compared among different models. A high expansion efficiency indicates that heat is being distributed into warmer (surface, tropical) water and a low value indicates that heat is being distributed into colder (deeper, high latitude) water.

The present model's water mass changes are probably less reliable than its steric expansion. The model predicts increased snow fall on the ice sheets, with even greater melting around their edges, which seems reasonable. However, the greatest uncertainty is a possible change in glacial ice dynamics (such as a collapse of the West Antarctic ice sheet) which the model cannot simulate. Smaller sources of uncertainty lie in the model's fixed lake and glacial ice areas, the behavior of grid cells without a river outlet, the absence of dams, and ground water withdrawals.

As stated by Bryan [1996]: "The most useful aspect of using a general circulation model of the ocean to estimate sea level rise is a prediction of the spatial distribution of the sea level rise." Until different models can show similar patterns of sea level rise, confidence in the patterns must remain low. The complicated derivation of sea level by Gregory [1993] and Bryan is obtained more directly and precisely in the present mass conserving model, which, however, has its own known and unknown deficiencies.

Additional quantities and data of these simulations are available at our web site at: http://aom.giss.nasa.gov .

References

Abramopoulos F, Rosenzweig C, Choudhury B (1988) Improved ground hydrology calculations for global climate models (GCMs): soil water movements and evapotranspiration. J. Climate, 1, 921-941.

Bryan K (1996) The steric component of sea level rise associated with enhanced greenhouse warming: a model study. Clim. Dyn., 12, 545-555.

Cubasch U, Hegerl GC, Hellbach A, Hock H, Mikolajewicz U, Santer BD, Ross R (1995) A climate change simulation starting from 1935. Clim. Dyn., 11 (2), 71-84.

DeWolde JR, Huybrechts P, Oerlemans J, Van der Wal RSW (1997) Projections of global mean sea level rise calculated with a 2d energy-balance climate model and dynamic ice sheet models. Tellus, 49A, 486-502.

Fofonoff NP, Millard RC (1983) Computation of fundamental properties of seawater. UNESCO, Technical Papers in Marine Science, 44.

Gornitz V (1995a) Monitoring sea level changes. Climatic Change, 31, 515-544.

Gornitz V (1995b) A comparison of differences between recent and late Holocene sea-level trends from eastern North America and other selected regions. J. Coast. Res. Spec., Issue No. 17, 287-297.

Gornitz V, Lebedeff S (1987). Global sea level changes during the past century. In Sea Level Fluctuations and Coastal Evolution, Nummedal D, Pilkey OH, Howard JD (eds.). SEPM, Spec. Publ. 41, 3-16.

Gornitz V, Rosenzweig C, Hillel D (1997) Effects of anthropogenic intervention in the land hydrologic cycle on global sea level rise. Glob. Planet. Change, 14, 147-161.

Gornitz V, Solow A (1991) Observations of long-term tide-gauge records for indicators of accelerated sea-level rise. In Greenhouse-Gas-Induced Climatic Change: A Critical Appraisal of Simulations and Observations, Schlesinger ME (ed.). Elsevier, Amsterdam, 347-367 pp.

Gregory JM (1993) Sea level changes under increasing atmospheric CO_2 in a transient coupled ocean-atmosphere GCM experiment. J. Climate, 6, 2247-2262.

Hansen JE, Sato M, Lacis A, Ruedy R, Tegan I, Matthews E, (1998) Climate forcings in the industrial era. Proc. Natl. Acad. Sci., 95, 12753-12758.

Houghton JT, Meira Filho LG, Callander BA, Harris N, Kattenberg A, Maskell K (eds.) (1996) Climate Change 1995: The Science of Climate Change. Cambridge University Press, 567 pp.

Hurrell JW (1995) Decadal trends in the North Atlantic Oscillation: regional temperatures and precipitation. Science, 269, 676-679.

Komar PD, Enfield DB (1987) Short-term sea level changes and shore-line erosion. In Sea Level Fluctuations and Coastal Evolution, Nummedal D, Pilkey OH, Howard JD (eds.). SEPM, Spec. Publ. 41, 17-27.

Large WG, McWilliams JC, Doney SC (1994) Oceanic vertical mixing: review and a model with non-local boundary layer parameterization. Rev. Geophys., 32, 363-403.

Levitus S, Burgett R, Boyer TP (1994) World ocean atlas 1994. U.S. Department of Commerce, NOAA, Washington, D.C.

Maul GA, Hanson K (1991) Interannual coherence between North Atlantic atmospheric surface pressure and composite southern U.S.A. sea level. Geophys. Res. Lett., 18, 653-656.

Nerem RS (1999) Measuring very low frequency sea level variations using satellite altimeter data. Glob. Planet. Change, 20, 157-171.

Peltier WR (1999) Global sea level rise and glacial isostatic adjustment. Glob. Planet. Change, 20, 93-123.

Peltier WR, Tushingham AM (1991) Global sea level rise and the greenhouse effect: might they be connected. Science, 244, 806-810.

Pirazzoli PA (1991) World Atlas of Holocene Sea-Level Changes. Elsevier, Amsterdam, 300 pp.

Raper SCB, Wigley TML, Warrick RA (1996) Global sea-level rise: past and future. In Sea Level Rise and Coastal Subsidence, Causes, and Consequences and Strategies, Milliman JD, Haq BU (eds.). Kluwer Academic Publishers, Dordrecht, 369 pp.

Russell GL, Miller JR, Rind D, Ruedy RA, Schmidt GA, Sheth S, (1999) Comparison of model and observed regional temperature changes during the past 40 years. Submitted to J. Geophys. Res.

Russell GL, Miller JR, Rind D (1995) A coupled atmosphere-ocean model for transient climate change studies. Atmos.-Ocean, 33(4), 683-730.

Spencer NE, Woodworth PL (1993). Data holdings of the Permanent Service for Mean Sea Level. PSMSL, Bidston Observatory, Birkenhead, U.K., 81 pp.

Warrick RA, LeProvost C, Meier MF, Oerlemans J, Woodworth PL, (1996) In Climate Change 1995: The Science of Climate Change, Houghton JT, Meira Hilho LG, Callander BA, Harris N, Kattenberg A, Maskell K (eds.). Cambridge University Press, 567 pp.

Table 1. Tide gauge station name, longitude, latitude, years of record, raw tide gauge trend (mm/year) for all years of the record [Spencer and Woodworth, 1993], geologic trend due to land motions, corrected tide gauge trend for all years of the record, corrected tide gauge trend for years 1960 to present, and model sea level trends for each GHG experiment from 1960 until the end of the observational record. The trends, other than the geologic trend, are calculated from a least squares fit line of the data in Figure 1.

City	Long,Lat	Ymin	Ymax	Raw Tide	Geol	Corr All	Corr 1960	GHG1	GHG2
Auckland	175E,35S	1904	1988	1.35	-.1	1.45	.01	1.68	1.78
Balboa	80W, 9N	1908	1995	1.34	1.7	-.36	-.85	1.28	.94
Bombay	73E,19N	1878	1992	.76	0.	.76	.25	2.04	1.77
Brest	5W,48N	1807	1996	.96	.15	.81	.94	1.53	2.46
Buenos Aires	58W,35S	1905	1987	1.57	0.	1.57	4.79	1.55	2.07
Churchill	94W,58N	1940	1994	-9.70	-9.8	.10	-4.39	2.39	2.18
Halifax	64W,45N	1920	1996	3.36	2.83	.53	-.60	1.13	1.08
Honolulu	158W,21N	1905	1997	1.55	.3	1.25	1.33	.52	.99
Key West	82W,25N	1913	1997	2.23	.69	1.54	1.99	1.44	1.33
Marseille	5E,43N	1885	1996	1.22	.75	.47	-1.01	1.18	1.80
New York	74W,41N	1856	1996	2.72	2.17	.55	.09	2.53	1.91
Prince Rupert	130W,54N	1909	1996	1.07	.4	.67	.89	.93	1.98
San Francisco	122W,38N	1855	1997	1.41	1.5	-.09	1.14	1.40	1.75
Stavanger	5E,59N	1882	1997	.13	-1.8	1.93	1.92	2.75	2.90
Stockholm	18E,59N	1889	1997	-3.92	-4.5	.58	1.55	3.04	2.43
Sydney	151E,34S	1897	1993	.68	-.3	.98	1.04	.76	2.74
Victoria	124W,48N	1910	1996	.74	0.	.74	1.02	1.16	1.50

Table 2. Changes in ocean surface height (mm/year) and its components for each GHG experiment minus the appropriate control simulation. The fourth line is the change in net heat into the ocean (W/m^2). The fifth line is the expansion efficiency of heat ($m^3/kW \cdot year$), calculated as the ratio of the second and fourth lines.

	1950-1999		2000-2049		2050-2099	
	GHG1	GHG2	GHG1	GHG2	GHG1	GHG2
Ocean Surface Ht.	1.15	1.29	2.83	3.04	5.55	4.95
Thermal Expansion	.83	.81	1.91	2.13	3.17	3.00
Water Mass Change	.32	.47	.92	.91	2.38	1.95
Net Heat into Ocean	.55	.51	1.36	1.45	2.19	2.05
Expansion Efficiency	1.50	1.59	1.41	1.47	1.45	1.47

Table 3. Changes in global water reservoirs in units of sea level rise (mm/year) for each GHG experiment minus the appropriate control simulation.

	1950-1999		2000-2049		2050-2100	
	GHG1	GHG2	GHG1	GHG2	GHG1	GHG2
Water Vapor	.03	.03	.03	.05	.04	.06
Snow on Ground	-.08	-.13	-.41	-.12	-.42	-.23
Land Ice	-.25	-.40	-.77	-1.02	-2.33	-2.18
Lake Mass	-.02	.02	.23	.20	.30	.37
Ocean + Sea Ice	.32	.47	.92	.91	2.38	1.95

Figure Captions

Figure 1. Separate graphs for each of 17 stations shows sea level changes integrated from 1950 for corrected tide gauge data and for each GHG experiments.

Figure 2. Integrated annual change in global sea level for each GHG experiment. Also shown are components due to thermal expansion and to water mass changes.

Figure 3. Expansion efficiency of heat as a function of temperature and pressure at a salinity of 35 per mil.

Figure 4. Spatial distribution of total sea level change for 2050 to 2099 minus 1950 for the average of the two GHG experiments minus the control simulations.

Figure 5. Spatial distribution of steric expansion for 2050 to 2099 minus 1950 for the average of the two GHG experiments minus the control simulations.

Figure 6. Spatial distribution of ocean and sea ice mass changes for 2050 to 2099 minus 1950 for the average of the two GHG experiments minus the control simulations.

Figure 7. Spatial distribution of continental water reservoir changes for 2050 to 2099 minus 1950 for the average of the two GHG experiments minus the control simulations. Also shown is the first letter of each station name located in the ocean cell from which model data comes.

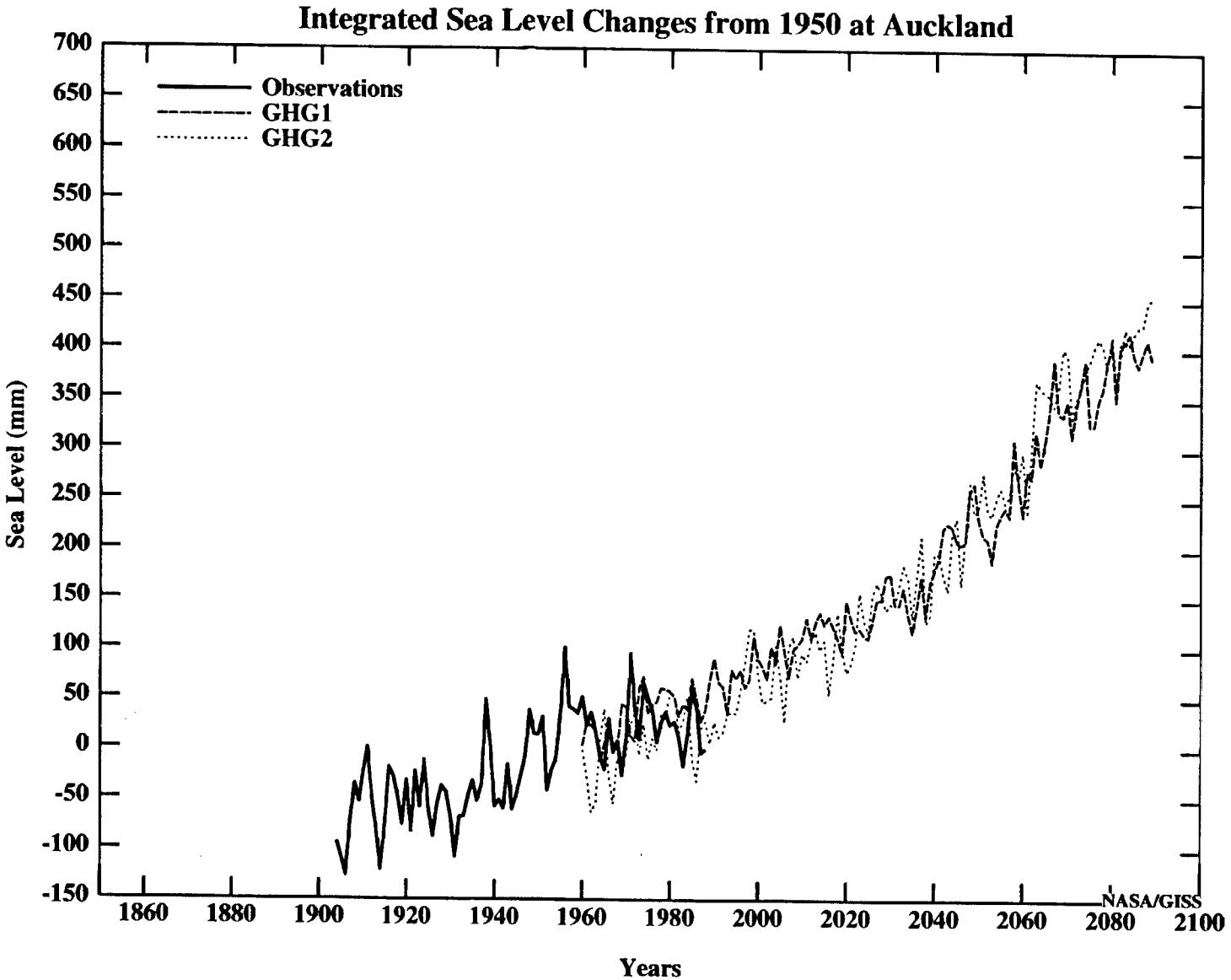
Integrated Sea Level Changes from 1950 at Auckland
Observations
GHG1
GHG2
Sea Level (mm)
700
650
600
550
500
450
400
350
300
250
200
150
100
50
0
-50
-100
-150
1860
1880
1900
1920
1940
1960
1980
2000
2020
2040
2060
2080
2100
Years
NASA/GISS

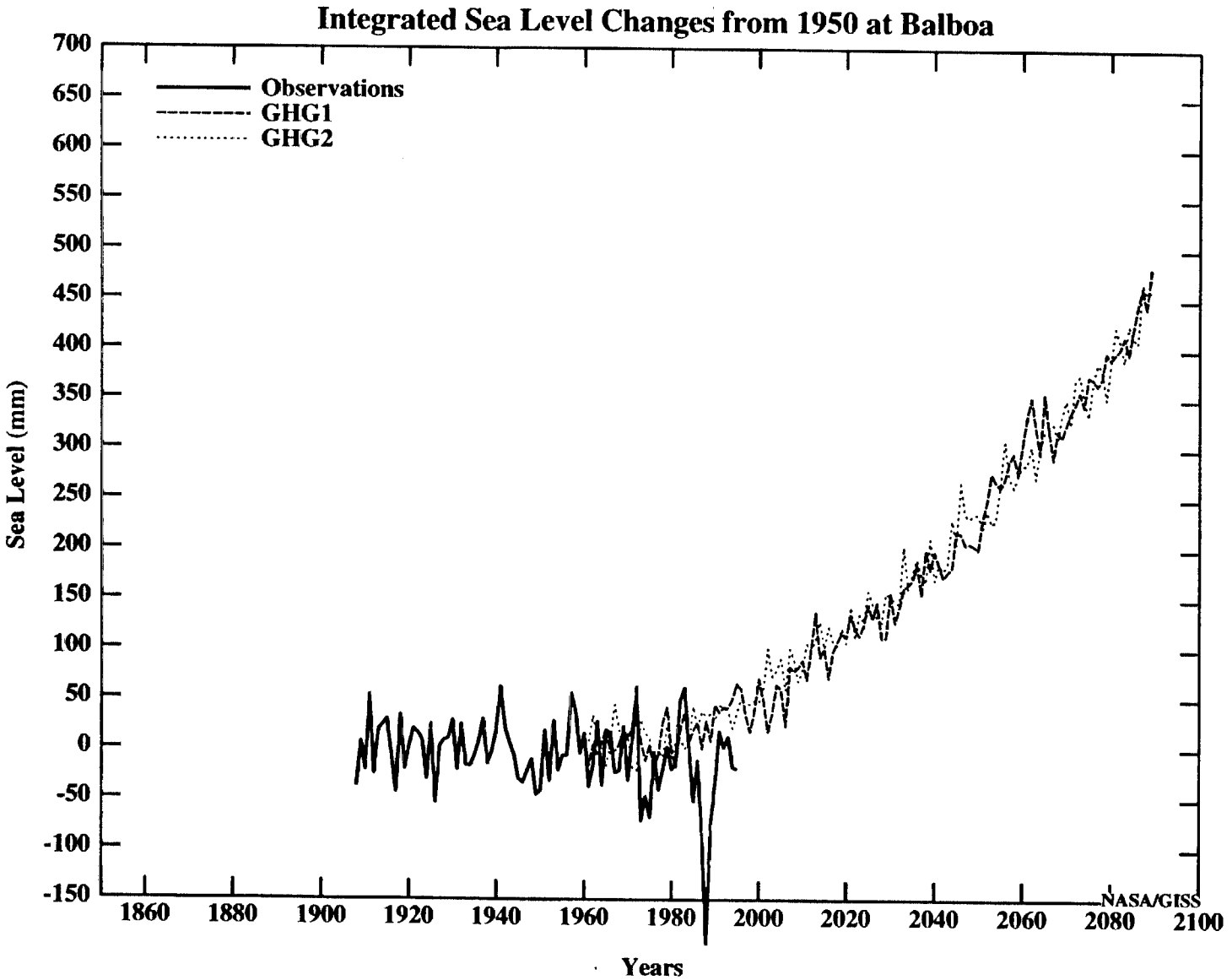
Integrated Sea Level Changes from 1950 at Balboa
Observations
GHG1
GHG2
Sea Level (mm)
700
650
600
550
500
450
400
350
300
250
200
150
100
50
0
-50
-100
-150
1860
1880
1900
1920
1940
1960
1980
2000
2020
2040
2060
2080
2100
Years
NASA/GISS

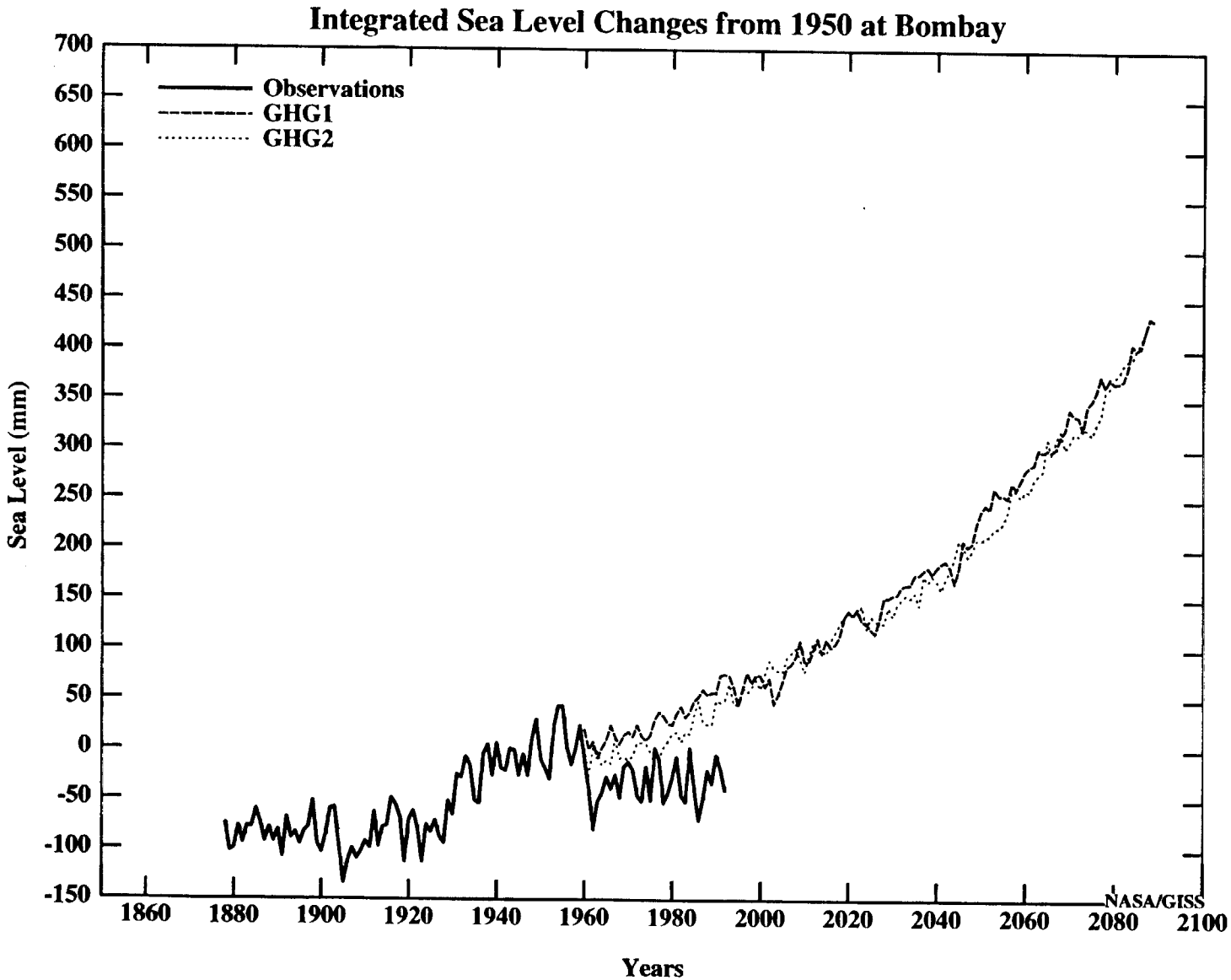
Integrated Sea Level Changes from 1950 at Bombay
Observations
GHG1
GHG2
Sea Level (mm)
700
650
600
550
500
450
400
350
300
250
200
150
100
50
0
-50
-100
-150
1860
1880
1900
1920
1940
1960
1980
2000
2020
2040
2060
2080
2100
Years
NASA/GISS

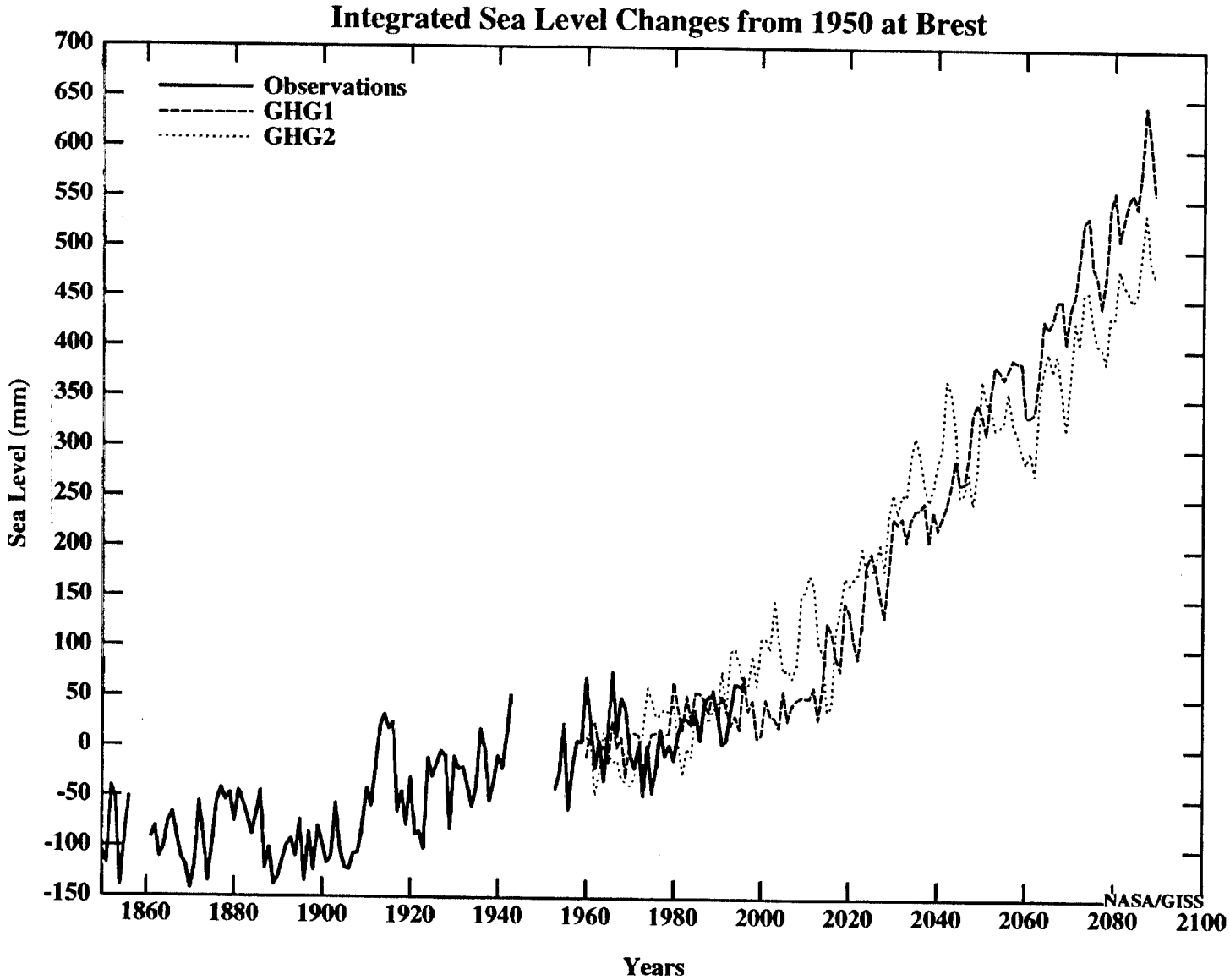
Integrated Sea Level Changes from 1950 at Brest
Observations
GHG1
GHG2
Sea Level (mm)
700
650
600
550
500
450
400
350
300
250
200
150
100
50
0
-50
-100
-150
1860
1880
1900
1920
1940
1960
1980
2000
2020
2040
2060
2080
2100
Years
NASA/GISS

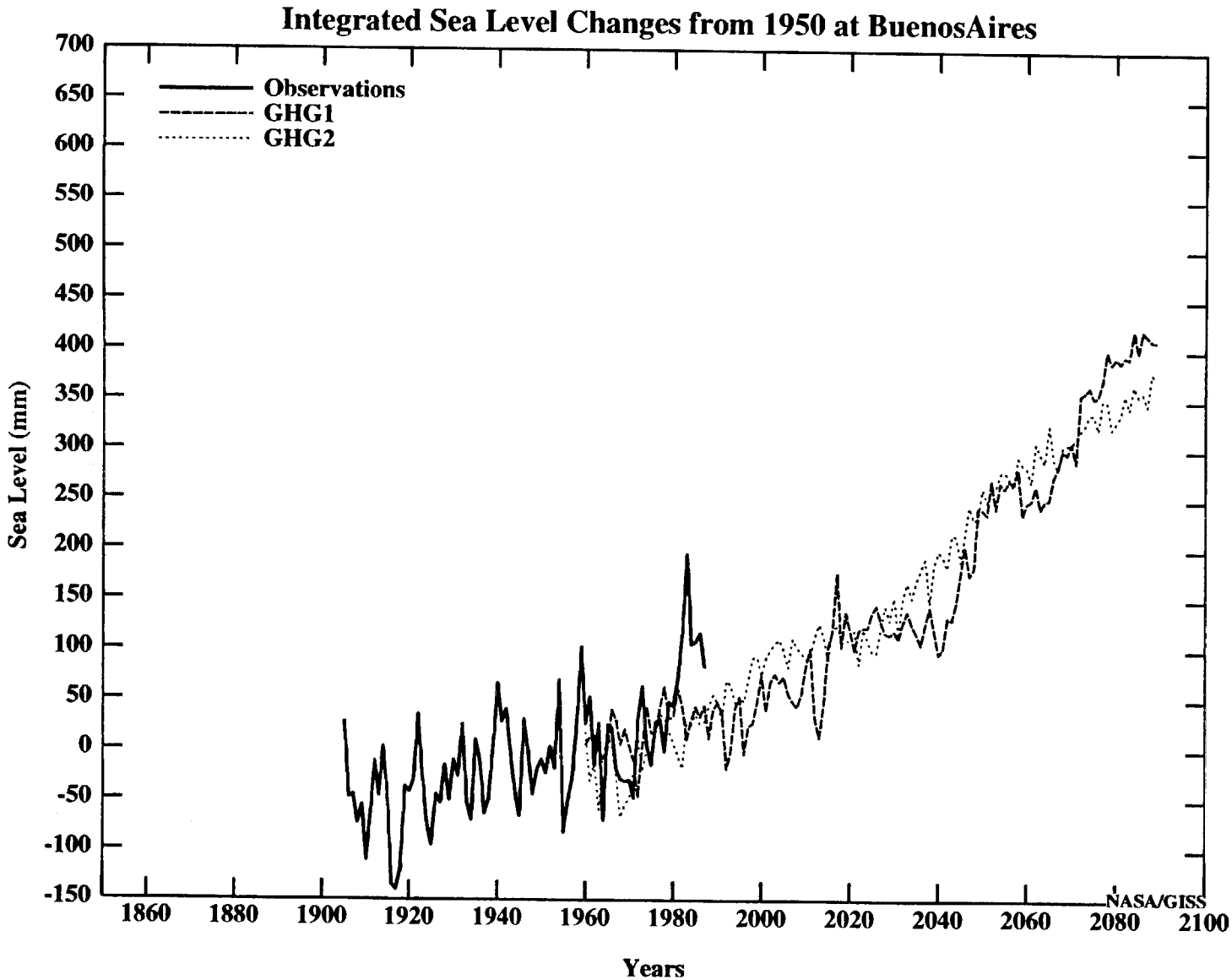
Integrated Sea Level Changes from 1950 at BuenosAires
Observations
GHG1
GHG2
Sea Level (mm)
700
650
600
550
500
450
400
350
300
250
200
150
100
50
0
-50
-100
-150
1860
1880
1900
1920
1940
1960
1980
2000
2020
2040
2060
2080
2100
Years
NASA/GISS

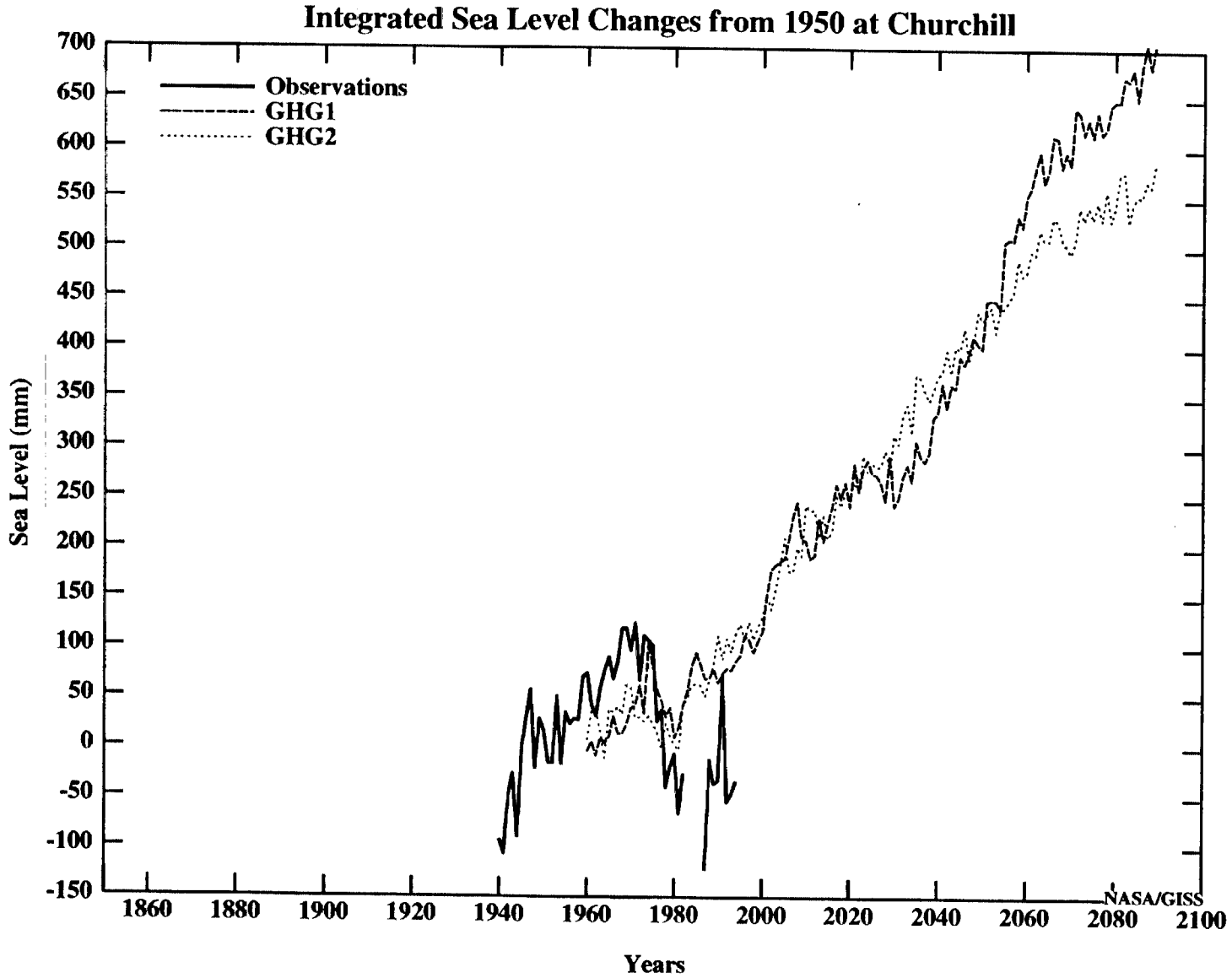
Integrated Sea Level Changes from 1950 at Churchill
Observations
GHG1
GHG2
Sea Level (mm)
700
650
600
550
500
450
400
350
300
250
200
150
100
50
0
-50
-100
-150
1860
1880
1900
1920
1940
1960
1980
2000
2020
2040
2060
2080
2100
Years
NASA/GISS

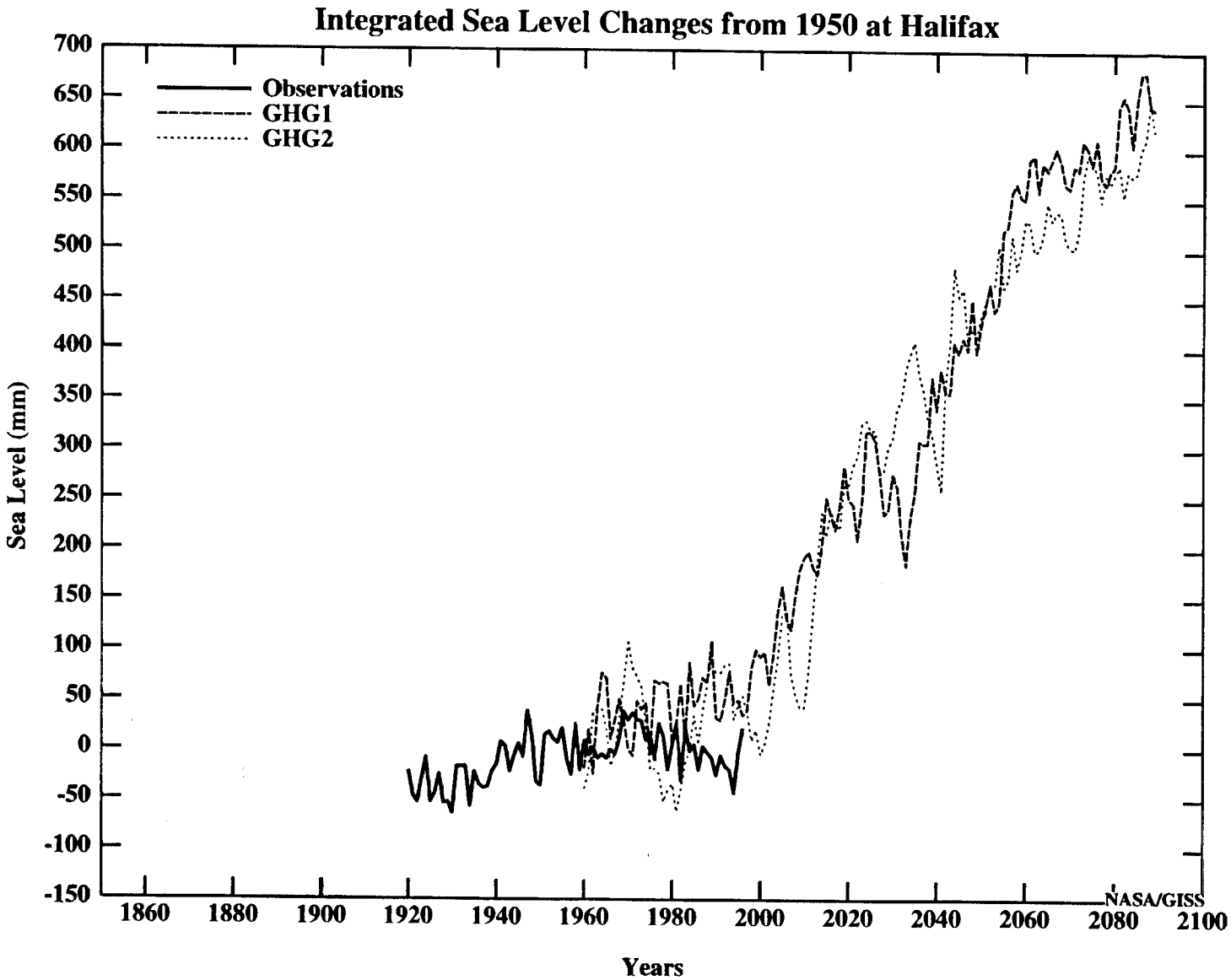
Integrated Sea Level Changes from 1950 at Halifax
Observations
GHG1
GHG2
Sea Level (mm)
700
650
600
550
500
450
400
350
300
250
200
150
100
50
0
-50
-100
-150
1860
1880
1900
1920
1940
1960
1980
2000
2020
2040
2060
2080
2100
Years
NASA/GISS

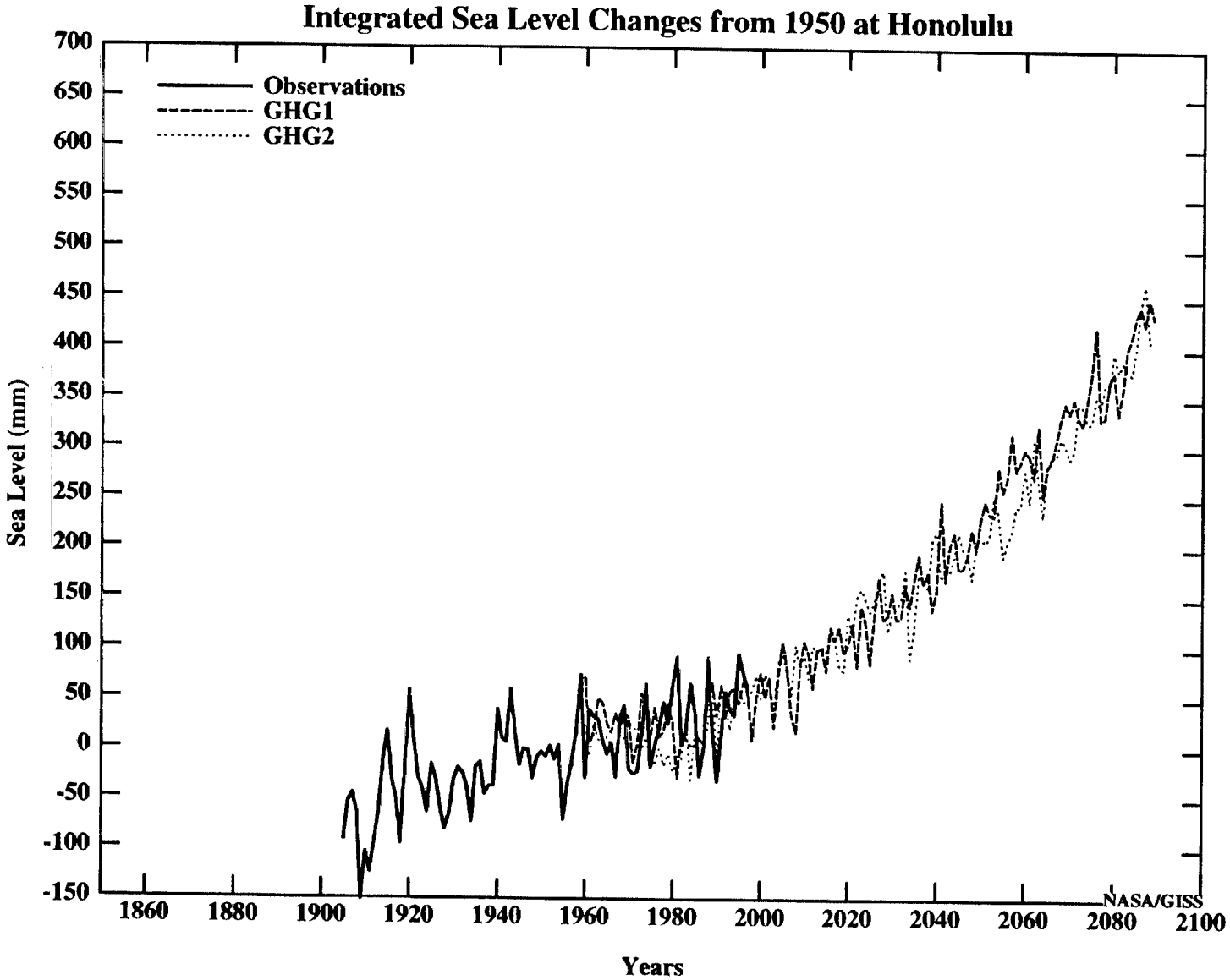
Integrated Sea Level Changes from 1950 at Honolulu
Observations
GHG1
GHG2
Sea Level (mm)
700
650
600
550
500
450
400
350
300
250
200
150
100
50
0
-50
-100
-150
1860
1880
1900
1920
1940
1960
1980
2000
2020
2040
2060
2080
2100
Years
NASA/GISS

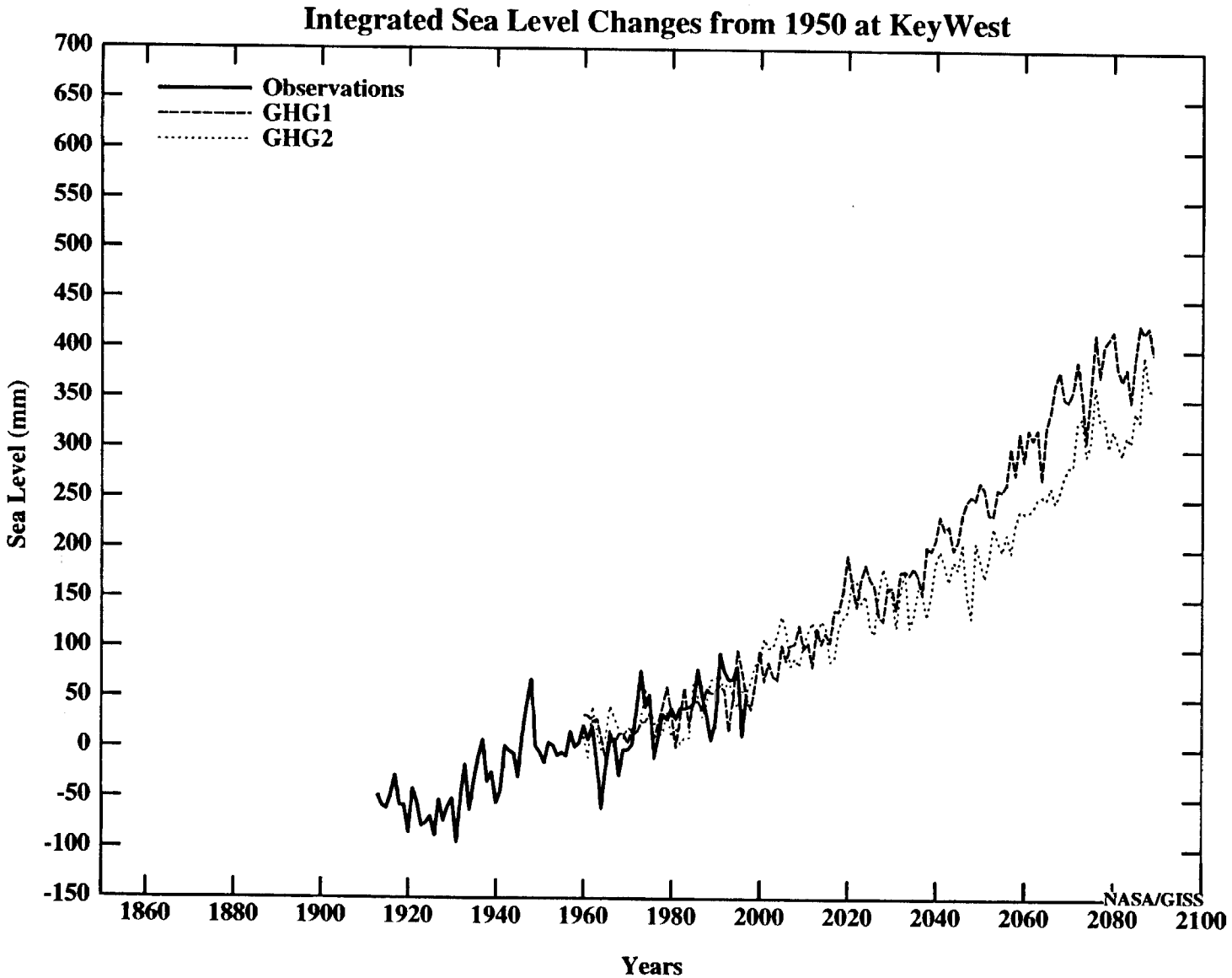
Integrated Sea Level Changes from 1950 at KeyWest
Observations
GHG1
GHG2
Sea Level (mm)
700
650
600
550
500
450
400
350
300
250
200
150
100
50
0
-50
-100
-150
1860
1880
1900
1920
1940
1960
1980
2000
2020
2040
2060
2080
2100
Years
NASA/GISS

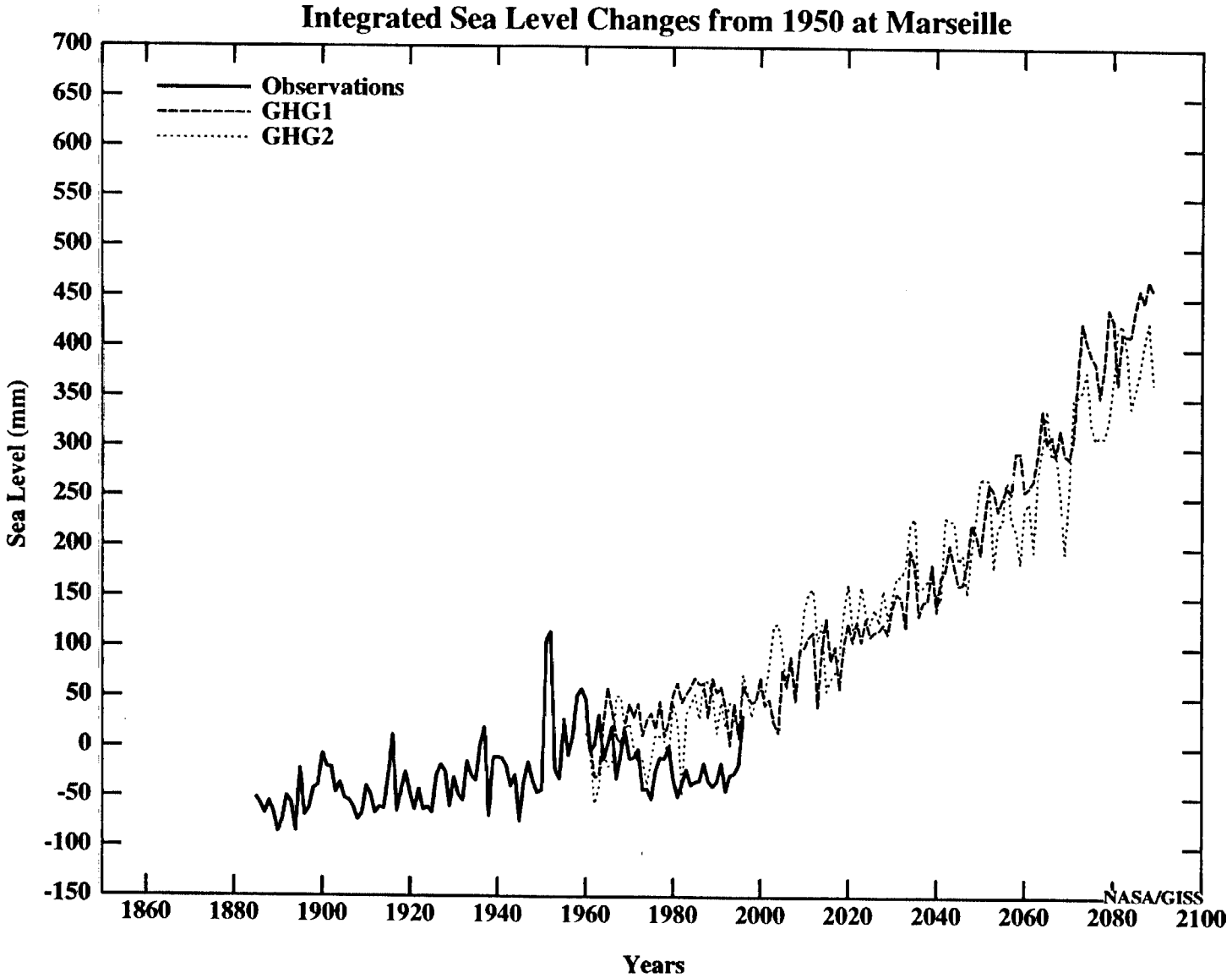
Integrated Sea Level Changes from 1950 at Marseille
Observations
GHG1
GHG2
Sea Level (mm)
700
650
600
550
500
450
400
350
300
250
200
150
100
50
0
-50
-100
-150
1860
1880
1900
1920
1940
1960
1980
2000
2020
2040
2060
2080
2100
Years
NASA/GISS

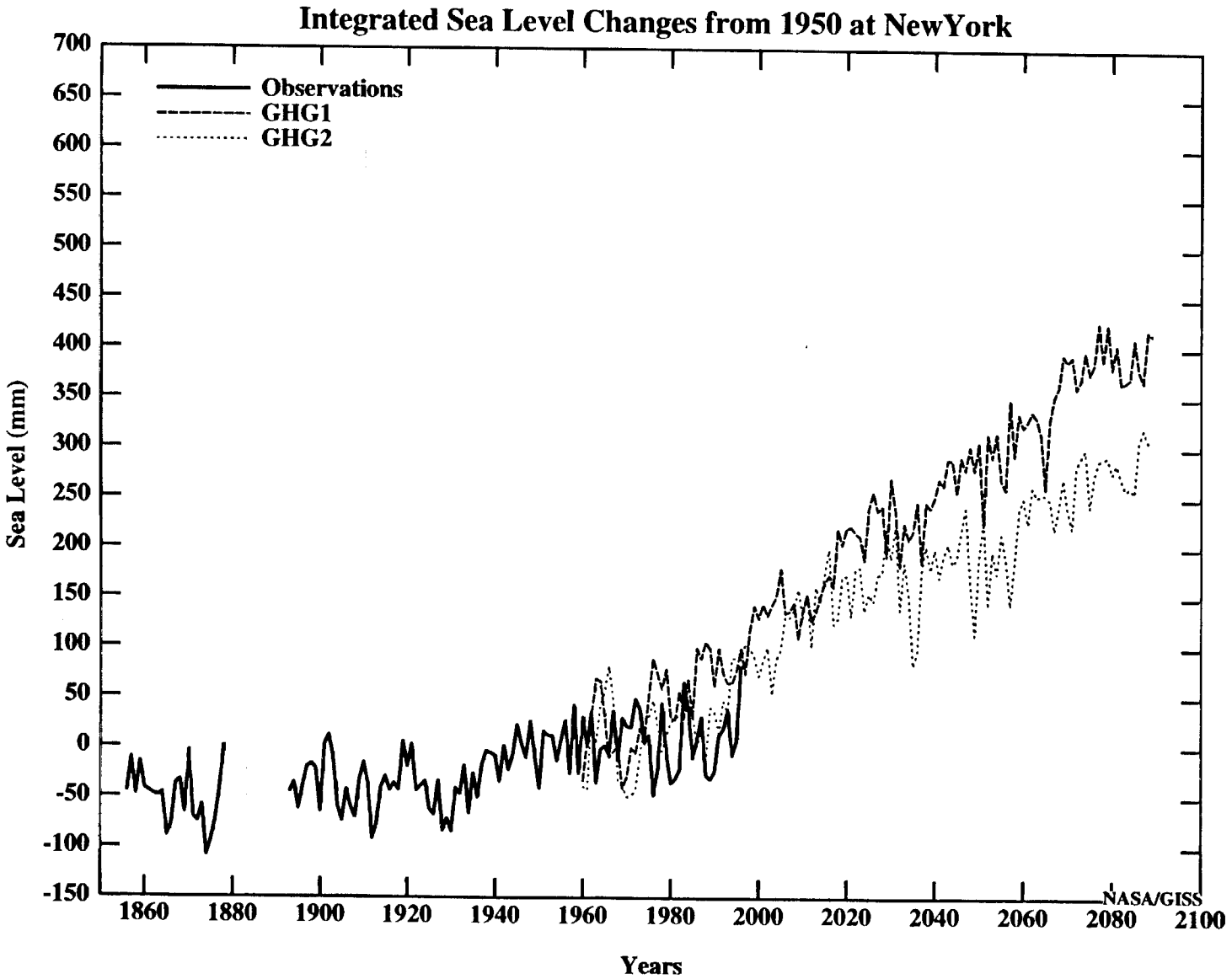
Integrated Sea Level Changes from 1950 at NewYork
Observations
GHG1
GHG2
Sea Level (mm)
700
650
600
550
500
450
400
350
300
250
200
150
100
50
0
-50
-100
-150
1860
1880
1900
1920
1940
1960
1980
2000
2020
2040
2060
2080
2100
Years
NASA/GISS

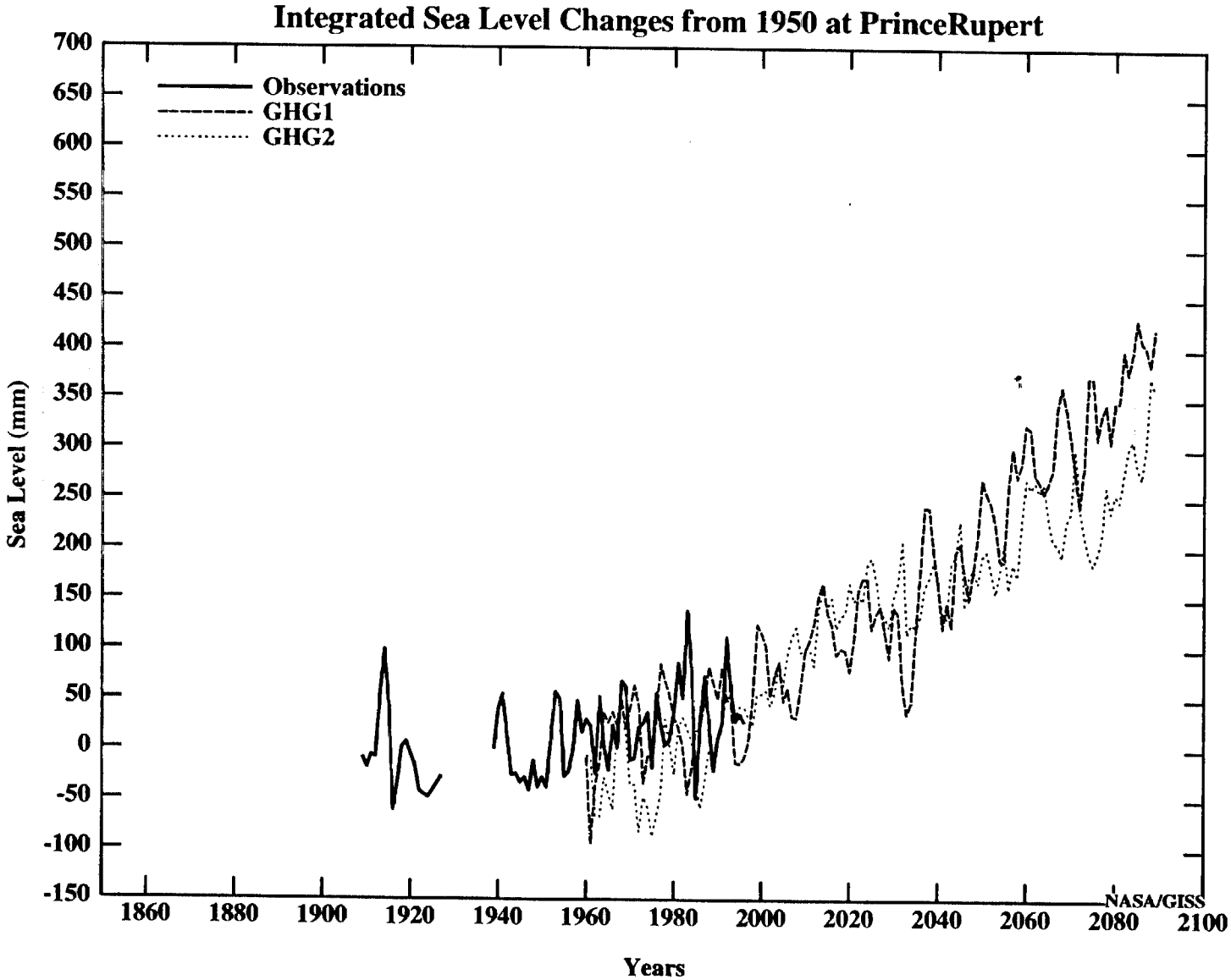
Integrated Sea Level Changes from 1950 at PrinceRupert
Observations
GHG1
GHG2
Sea Level (mm)
700
650
600
550
500
450
400
350
300
250
200
150
100
50
0
-50
-100
-150
1860
1880
1900
1920
1940
1960
1980
2000
2020
2040
2060
2080
2100
Years
NASA/GISS

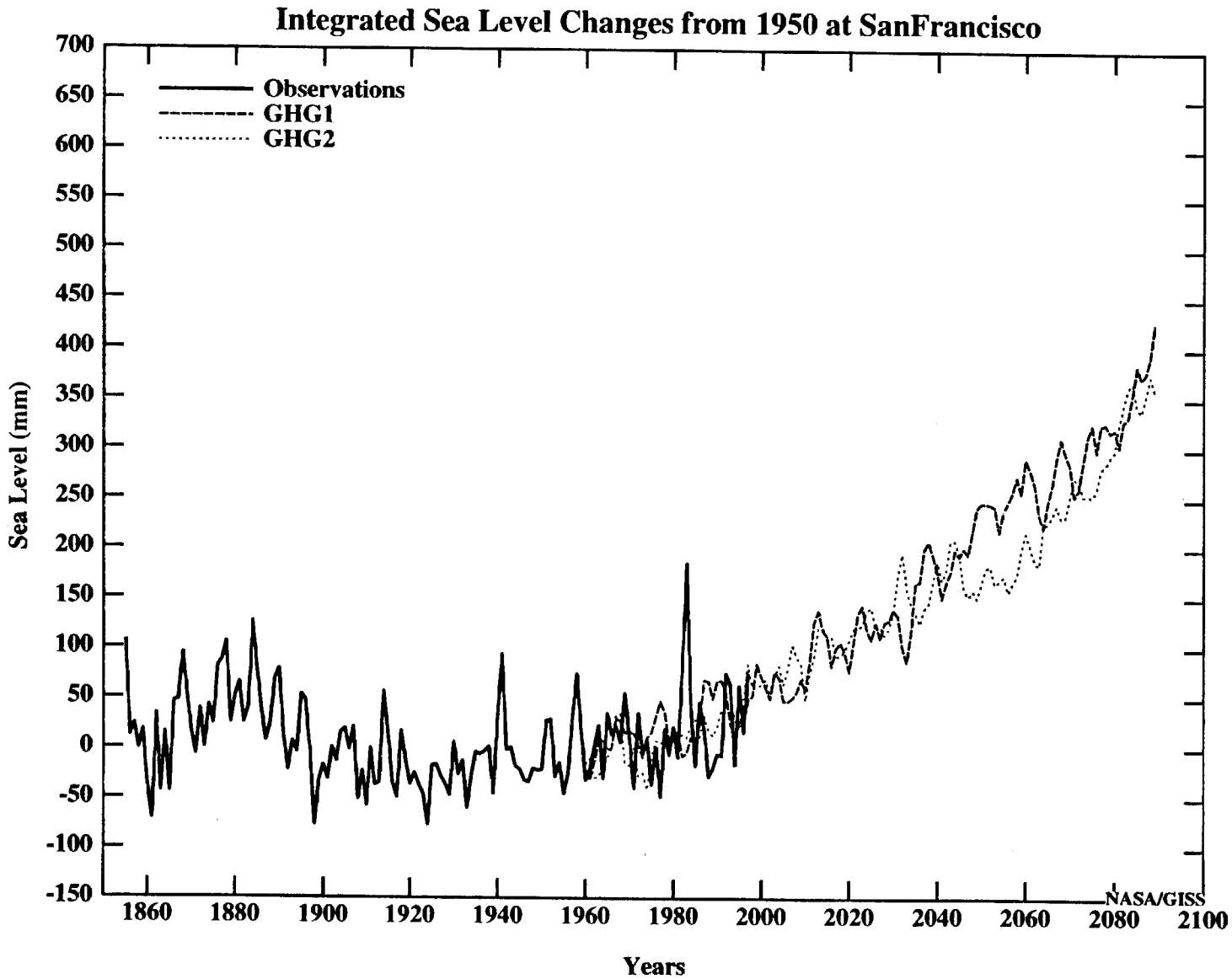
Integrated Sea Level Changes from 1950 at SanFrancisco
Observations
GHG1
GHG2
Sea Level (mm)
700
650
600
550
500
450
400
350
300
250
200
150
100
50
0
-50
-100
-150
1860
1880
1900
1920
1940
1960
1980
2000
2020
2040
2060
2080
2100
Years
NASA/GISS

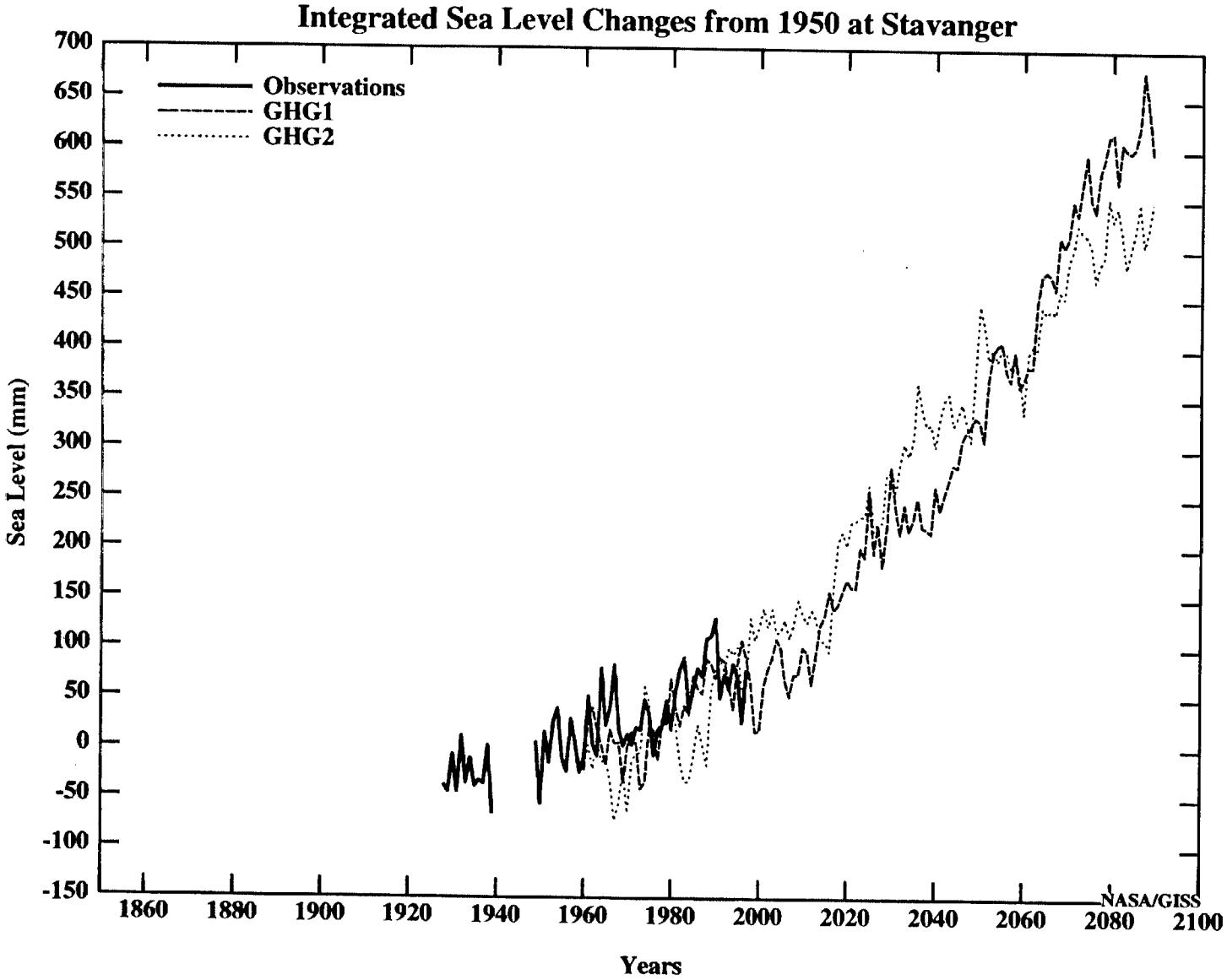
Integrated Sea Level Changes from 1950 at Stavanger
Observations
GHG1
GHG2
Sea Level (mm)
700
650
600
550
500
450
400
350
300
250
200
150
100
50
0
-50
-100
-150
1860
1880
1900
1920
1940
1960
1980
2000
2020
2040
2060
2080
2100
Years
NASA/GISS

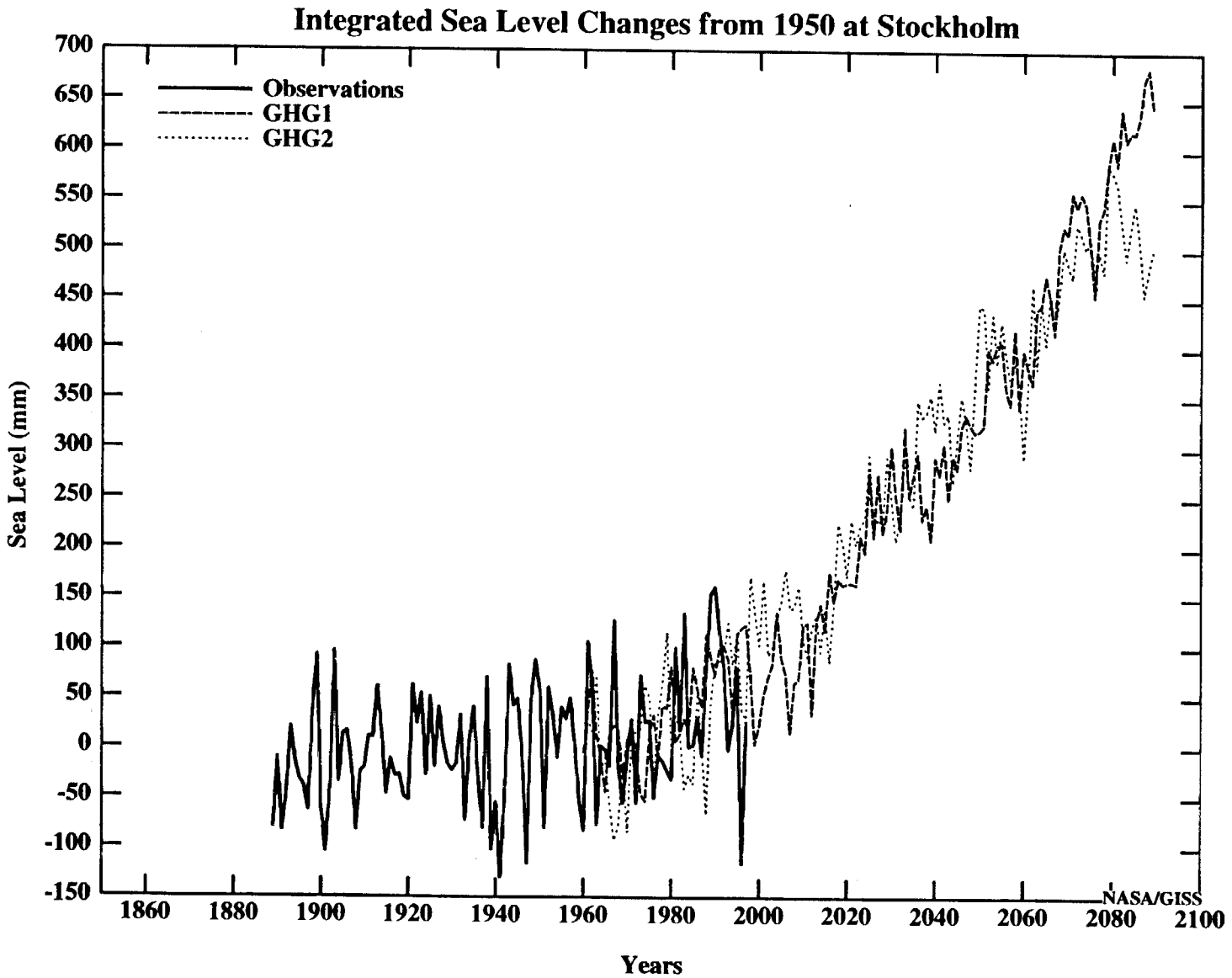
Integrated Sea Level Changes from 1950 at Stockholm
Observations
GHG1
GHG2
Sea Level (mm)
700
650
600
550
500
450
400
350
300
250
200
150
100
50
0
-50
-100
-150
1860
1880
1900
1920
1940
1960
1980
2000
2020
2040
2060
2080
2100
Years
NASA/GISS

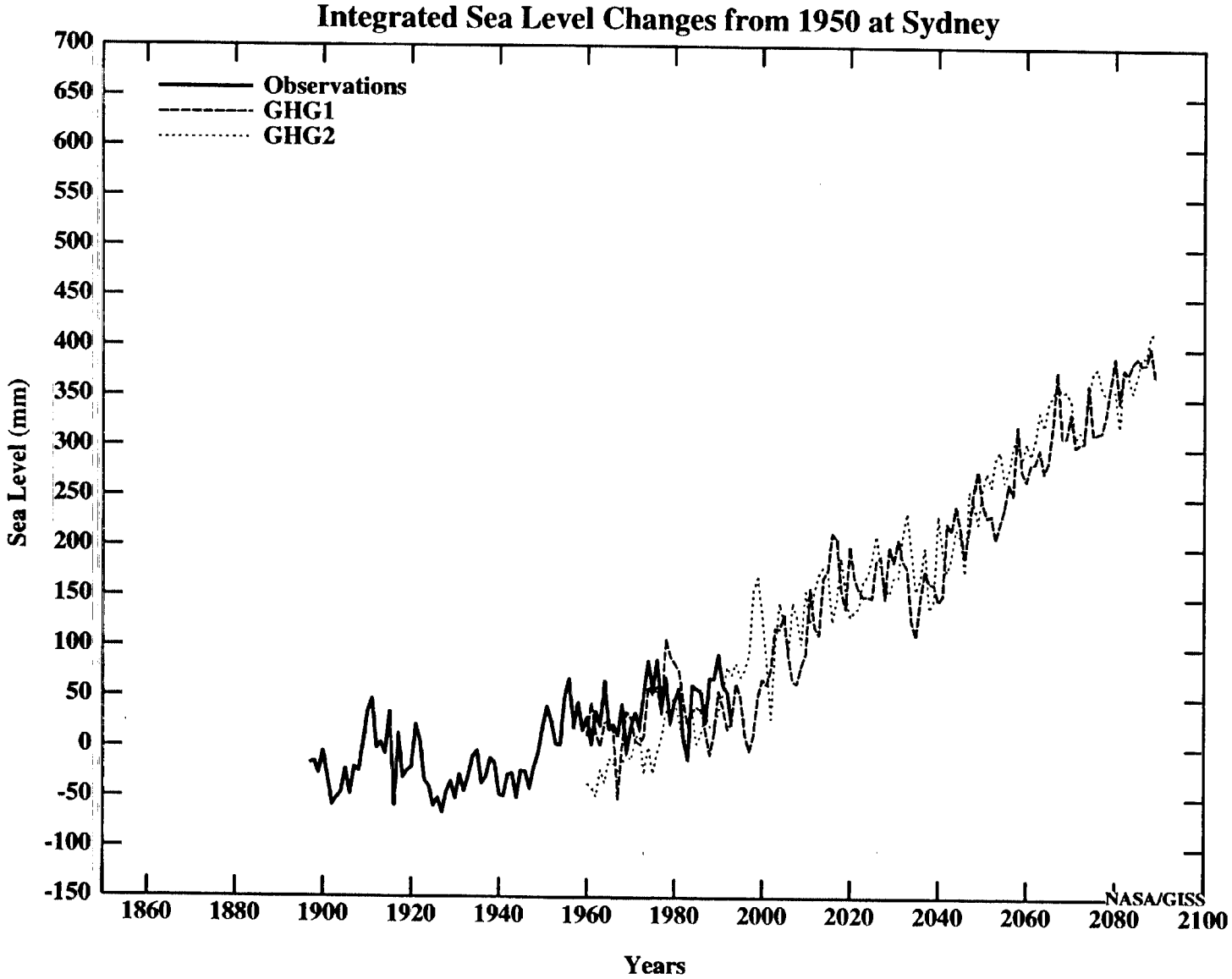
Integrated Sea Level Changes from 1950 at Sydney
Observations
GHG1
GHG2
Sea Level (mm)
700
650
600
550
500
450
400
350
300
250
200
150
100
50
0
-50
-100
-150
1860
1880
1900
1920
1940
1960
1980
2000
2020
2040
2060
2080
2100
Years
NASA/GISS

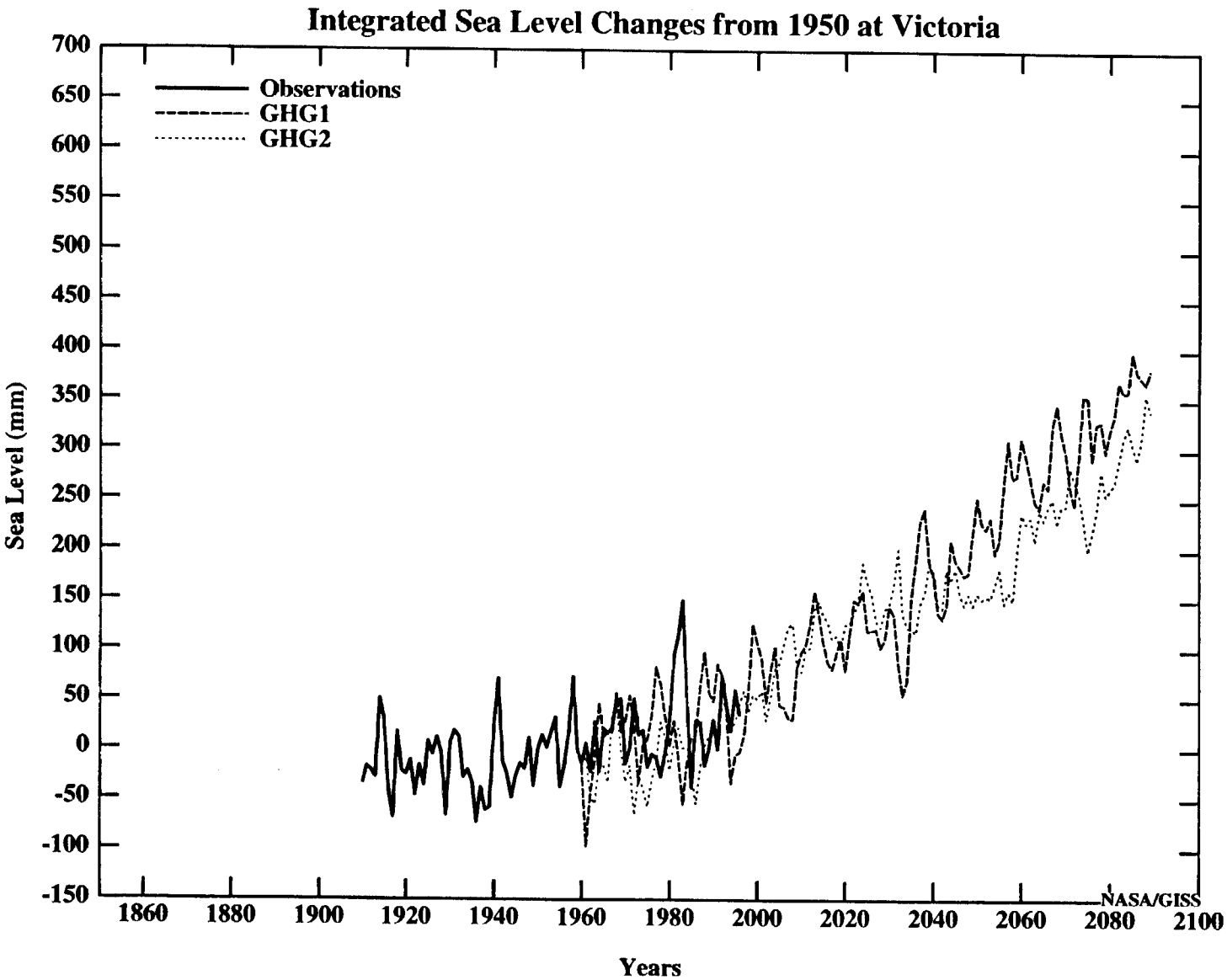
Integrated Sea Level Changes from 1950 at Victoria
Observations
GHG1
GHG2
Sea Level (mm)
700
650
600
550
500
450
400
350
300
250
200
150
100
50
0
-50
-100
-150
1860
1880
1900
1920
1940
1960
1980
2000
2020
2040
2060
2080
2100
Years
NASA/GISS

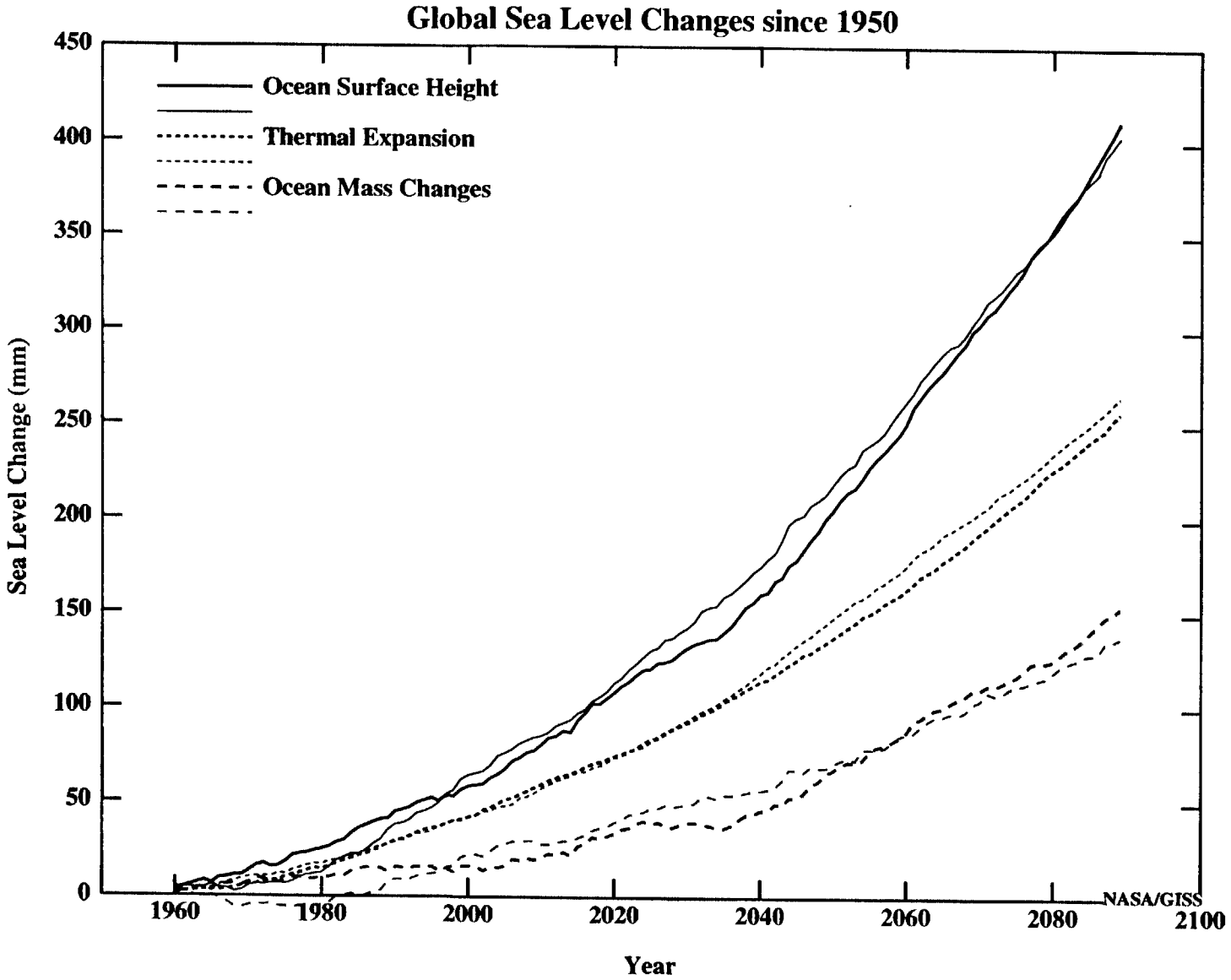
Global Sea Level Changes since 1950
Ocean Surface Height
Thermal Expansion
Ocean Mass Changes
Sea Level Change (mm)
450
400
350
300
250
200
150
100
50
0
1960
1980
2000
2020
2040
2060
2080
2100
Year
NASA/GISS

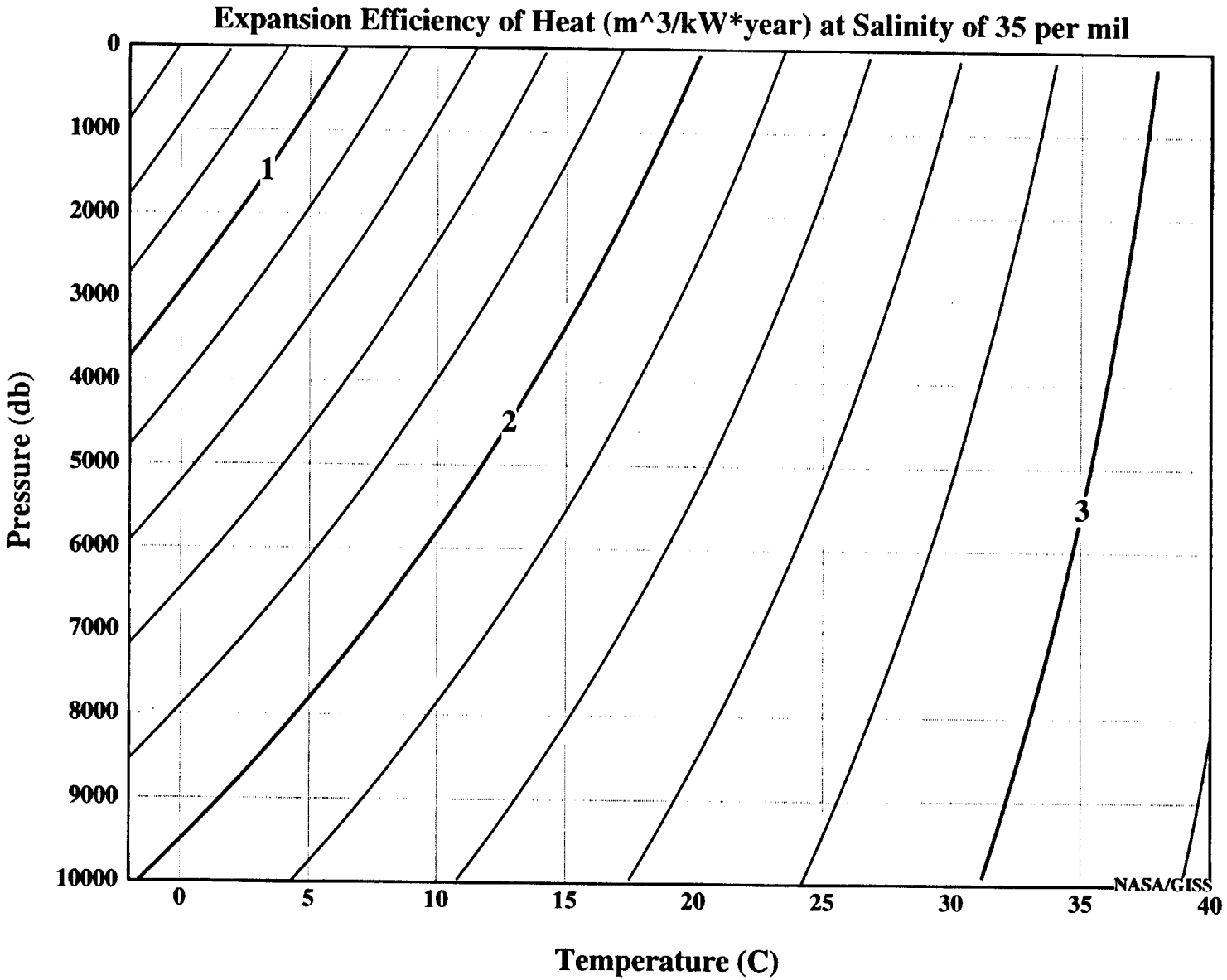
Expansion Efficiency of Heat (m^3/kW*year) at Salinity of 35 per mil
Pressure (db)
0
1000
2000
3000
4000
5000
6000
7000
8000
9000
10000
1
2
3
NASA/GISS
0
5
10
15
20
25
30
35
40
Temperature (C)

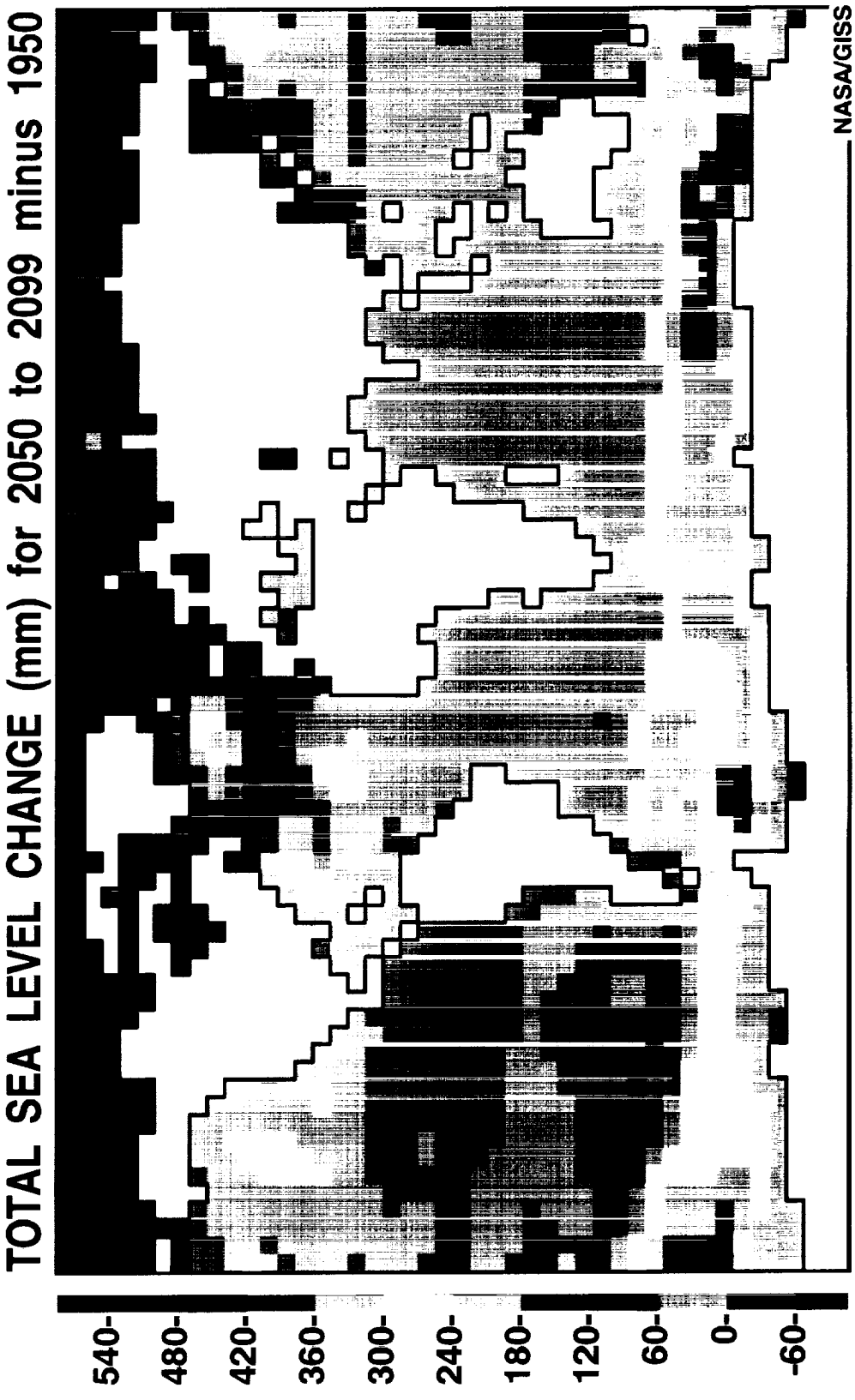
TOTAL SEA LEVEL CHANGE (mm) for 2050 to 2099 minus 1950
540
480
420
360
300
240
180
120
60
0
-60
NASA/GISS

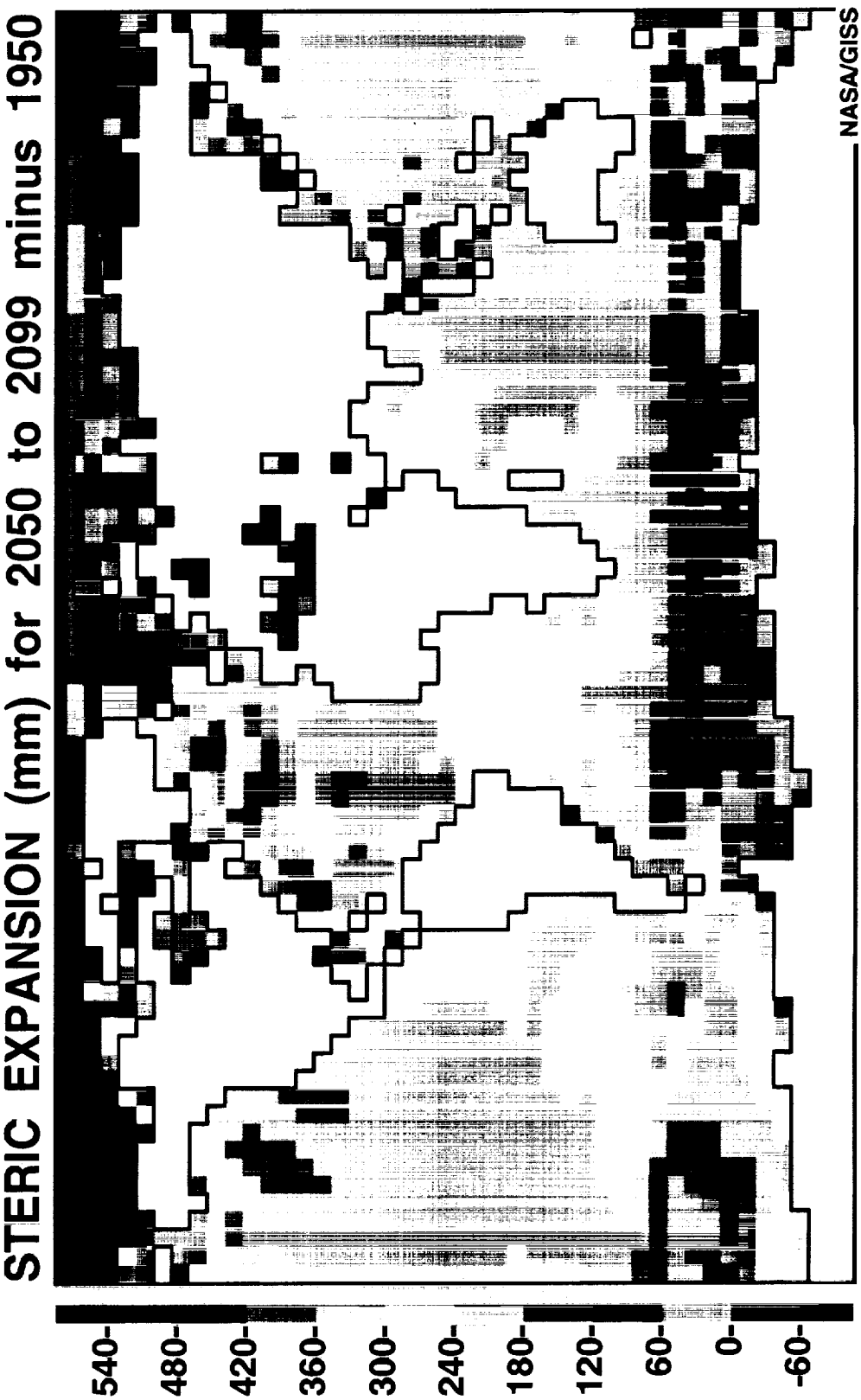
STERIC EXPANSION (mm) for 2050 to 2099 minus 1950
NASA/GISS
540
480
420
360
300
240
180
120
60
0
-60

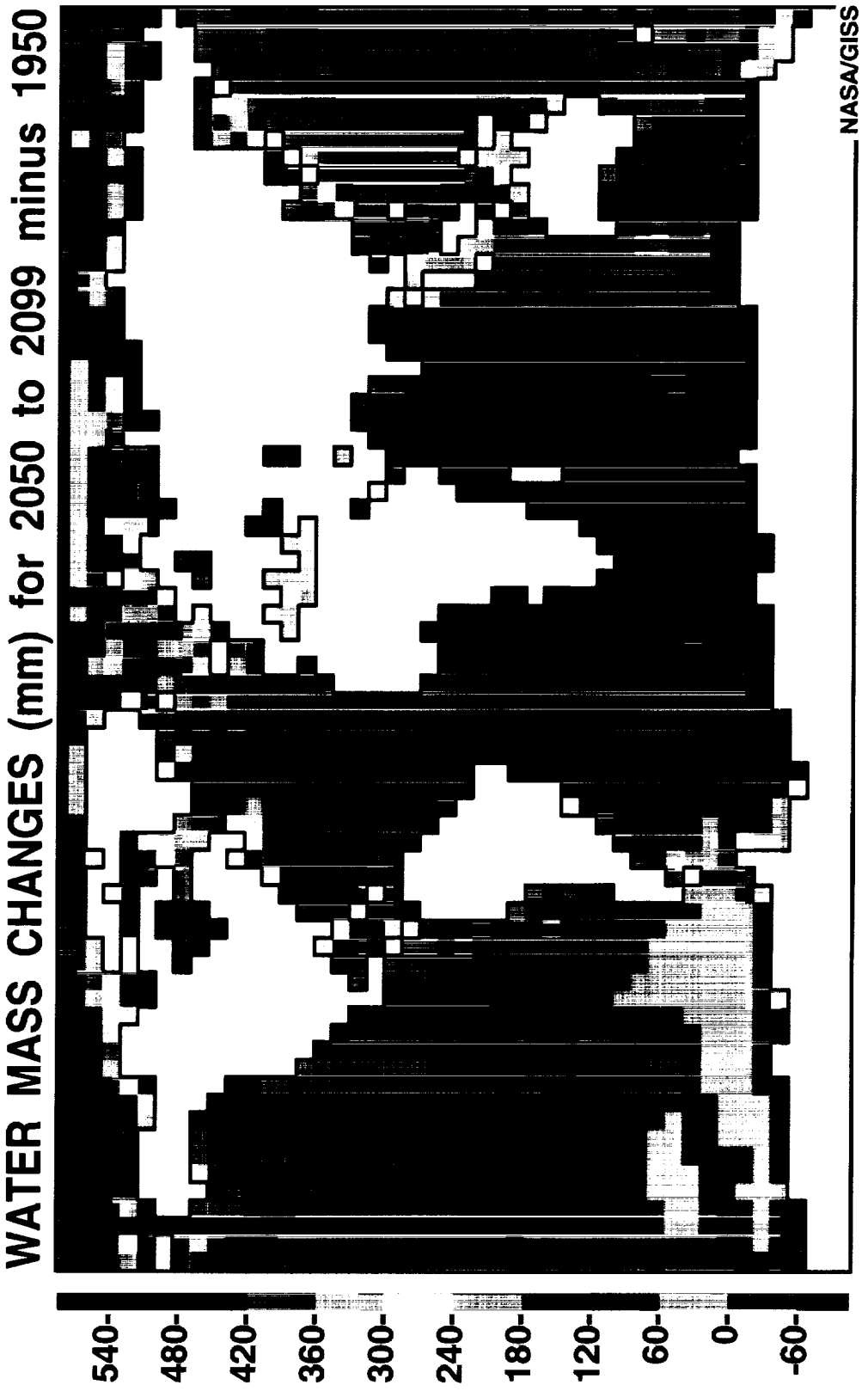
WATER MASS CHANGES (mm) for 2050 to 2099 minus 1950
540
480
420
360
300
240
180
120
60
0
-60
NASA/GISS

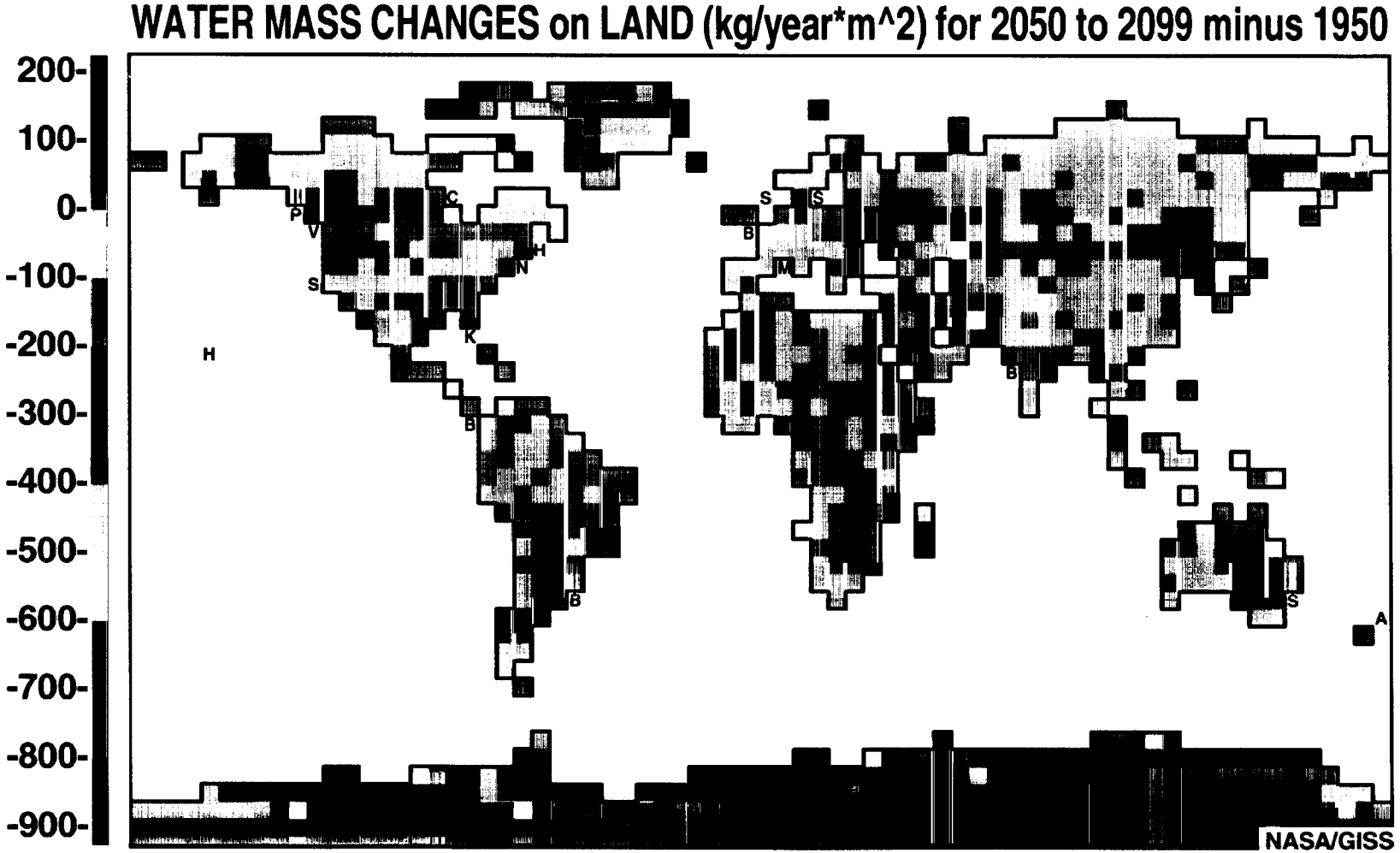
WATER MASS CHANGES on LAND (kg/year*m^2) for 2050 to 2099 minus 1950
200-
100-
0-
-100-
-200-
-300-
-400-
-500-
-600-
-700-
-800-
-900-
NASA/GISS